Composite pulses for optimal robust control in two-level systems

Hai-Ning Wu,[1,2] Cheng Zhang,[1,2] Jie Song,[3] Yan Xia,[1,2] and Zhi-Cheng Shi[1,2,*]
[1]*Fujian Key Laboratory of Quantum Information and Quantum Optics (Fuzhou University), Fuzhou 350108, China*
[2]*Department of Physics, Fuzhou University, Fuzhou 350108, China*
[3]*Department of Physics, Harbin Institute of Technology, Harbin 150001, China*

(Received 26 October 2022; accepted 23 January 2023; published 3 February 2023)

In this work, we put forward an approach of constructing the optimal composite pulse sequence for robust population transfer in two-level systems. This approach is quite universal and applicable to a variety of systems, because the modulation parameters of composite pulses are obtained by minimizing the homemade cost function rather than nullifying the error coefficients of the transition probability. Specifically, we design different forms of the cost function for implementing optimal robustness with respect to the single or multiple errors. When slightly adjusting the constraints of the cost function, this approach can be easily extended to achieve arbitrary population transfer. The numerical results demonstrate that the optimized sequences are immune from various systematic errors, allowing us to produce a broadening excitation range of the transition probability. Therefore, this work offers an optimal robust design for controlling quantum states in error-prone environments.

DOI: 10.1103/PhysRevA.107.023103

I. INTRODUCTION

Precise manipulation of quantum states is a topical subject in quantum information processing [1]. The manipulation precision is often hardly satisfactory in practice due to the existence of various systematic errors. Actually, these errors prevent the system from evolving along the desired path, causing the quantum state to deviate from the exact one. Hence, improving the robust performance of the system dynamics and thus reducing the influence of systematic errors becomes a very necessary issue.

To tackle this issue, several techniques have been proposed [2–11]. Among them, the adiabatic passage [12–16] is well established and successfully used for robust quantum control [17–19]. In the adiabatic passage, one needs to select an eigenstate of the system Hamiltonian as the evolution path. Then the initial state would adiabatically evolve along this selected path without any transitions to other eigenstates. Nevertheless, its effectiveness strictly relies on high-energy and long-duration fields [16]. In other words, the insensitivity to systematic errors is obtained at the expense of slow evolution speed and not very high fidelity. As promising substitutions, the composite pulse (CP) technique and the optimal control (OC) approach have attracted much attention due to their ultrahigh fidelity and robustness against systematic errors.

The concept of CPs was early conceived in polarized optics [20–24] and further developed in nuclear magnetic resonance (NMR) [25–27]. The CPs are generally constituted by a finite train of constant pulses with determined pulse areas and well-defined phases. A basic rule of this technique is to exploit the modulation parameters of each pulse to compensate for the influence caused by tiny errors [28–30], or make the system highly sensitive to parameter deviations [28,31]. So far, the CP technique has been very much in favor in different physical systems [31–43], including trapped ions [44–53], cold-atom interference [54–56], quantum dots [57–59], etc.

The OC approach is widely applied in various subject branches [60–70]. Its core idea is to optimize some predefined targets that hinge on the manner of the system evolution [71–75]. In a nutshell, the control fields are derived via searching the extremum (the maximization or minimization) of the field-dependent cost functional [76]. In particular, some extra constraints can be contained in the cost functional as desired if there exist additional limitations or expectations [75–77]. In recent years, the modern version of OC is mainly developed from the Pontryagin maximum principle [72,75], and has offered substantial support for quantum applications [78–80]. For instance, Van Damme *et al*. [81] derived the global robust optimal control strategies for population transfer in terms of energy and time minimum. Through combining with deep reinforcement learning [82,83], the optimal pulses can be constructed in a desired manner to achieve robust quantum state preparation [84–87].

Up to now, many CP works on robust quantum control have been proposed through modulating a single type of parameters, such as the phase [28,29,88–91], the coupling strength [92–95], or the detuning [96], while the remaining parameters are preset. Actually, all system parameters are available to be utilized for modulation. From this point of view, the preceding CP sequences [28–30,88–96] do not reach the efficiency limit in terms of robustness. In principle, to achieve optimal robustness against errors, one requires to make all physical quantities adjustable.

In this work, we propose an approach of constructing the CP sequence for high-fidelity population transfer with optimal robustness against systematic errors. This approach depends

*szc2014@yeah.net

on searching the minimum value of the cost functions, effectively avoiding the situation in which the error terms of the transition probability cannot be completely canceled or the number of pulses is limited. To attain the efficiency limit in terms of robustness, *all physical quantities*, including the phase, the pulse area, the coupling strength, and the detuning, are regarded as free modulation parameters. By properly designing the form of the cost functions, the optimal CP sequences show outstanding robustness against multiple kinds of systematic errors. In particular, it is also accessible to generate the optimal sequence for arbitrary population transfer by flexibly adjusting the constraints of the cost function. Compared with previous CP sequences [96–98], the current one provides better robustness against the pulse area error and the detuning error, and possesses a superior broad excitation range for the transition probability. As a by-product, arbitrary population transfer can be obtained in a robust way through merely modulating the phase difference of two pulses, while other parameters remain unchanged.

The rest of the paper is organized as followed. In Sec. II, we introduce the physical model, the construction of the cost function, and the search algorithm for finding optimal CPs. An intensive study of the cost function configuration is presented in Sec. III. Section IV focuses on the design of optimal CPs robust against various errors derived from the pulse area, the detuning, and the coupling strength. Then, we popularize the current optimal CPs when the system exhibits multiple types of errors. Subsequently, we demonstrate the construction process of CPs using arbitrary population transfer. In Sec. V, we make a brief comparison between the current optimal CPs and previous works [25,96–100]. A conclusion is given in Sec. VI.

II. THEORETICAL FRAMEWORK

Let us consider a two-level quantum system coherently driven by an external control field. The system dynamics is governed by the Schrödinger equation ($\hbar = 1$)

$$i\partial_t \boldsymbol{c}(t) = \boldsymbol{H}(t)\boldsymbol{c}(t), \tag{1}$$

where $\boldsymbol{c}(t) = [c_1(t), c_2(t)]^{\mathbf{T}}$ is the probability amplitude vector, the superscript $\mathbf{T}$ denotes vector transposition, and $c_n(t)$ is the probability amplitude of the state $|\psi_n\rangle$ $(n = 1, 2)$. The Hamiltonian has the following form:

$$\boldsymbol{H}(t) = \frac{1}{2}\begin{bmatrix} -\Delta(t) & \Omega(t)e^{i\theta(t)} \\ \Omega(t)e^{-i\theta(t)} & \Delta(t) \end{bmatrix}, \tag{2}$$

where $\Delta(t) = (\omega_0 - \omega)$ is the detuning between the Bohr transition frequency ω_0 and the control field frequency ω, $\Omega(t)$ is the coupling strength of the transition $|\psi_1\rangle \leftrightarrow |\psi_2\rangle$, and $\theta(t)$ is the phase shift applied to the control field.

The probability amplitude vector at the evolution time t relates to the initial time t_0 via the propagator $\boldsymbol{U}(\tau)$:

$$\boldsymbol{c}(t) = \boldsymbol{U}(\tau)\boldsymbol{c}(t_0), \tag{3}$$

where $\tau = (t - t_0)$ is the pulse duration. It is instructive to present the expression of $\boldsymbol{U}(\tau)$ when the Hamiltonian is time independent, and the form reads

$$\begin{aligned}\boldsymbol{U}(\tau) &= \begin{bmatrix} U_{11}(\tau) & U_{12}(\tau) \\ U_{21}(\tau) & U_{22}(\tau) \end{bmatrix} \\ &= \begin{bmatrix} \cos\frac{A}{2} + i\frac{\chi\sin\frac{A}{2}}{\sqrt{\chi^2+1}} & -i\frac{\sin\frac{A}{2}}{\sqrt{\chi^2+1}}e^{i\theta} \\ -i\frac{\sin\frac{A}{2}}{\sqrt{\chi^2+1}}e^{-i\theta} & \cos\frac{A}{2} - i\frac{\chi\sin\frac{A}{2}}{\sqrt{\chi^2+1}} \end{bmatrix},\end{aligned} \tag{4}$$

with $\chi = \Delta/\Omega$ and the pulse area $A = \Omega\sqrt{\chi^2 + 1}\,\tau$. According to the expression of χ, it can be seen that two physical quantities Ω and Δ are not independent of each other in the propagator $\boldsymbol{U}(\tau)$. That is, we cannot simultaneously regard Ω and Δ as the free control parameters. In the following, we set the coupling strength Ω of each pulse as unit, and thus $\chi = \Delta$.

Assume that the system is initially in the state $|\psi_1\rangle$, i.e., $\boldsymbol{c}(0) = [1, 0]^{\mathbf{T}}$. The probability amplitude vector at the evolution time t becomes $\boldsymbol{c}(\tau) = [U_{11}(\tau), U_{21}(\tau)]^{\mathbf{T}}$. Thus, the transition probability of the state $|\psi_2\rangle$ reads

$$P = |U_{21}(\tau)|^2 = \frac{1}{\Delta^2 + 1}\sin^2\frac{A}{2}. \tag{5}$$

It is readily found that the transition probability P relies on the parameters Δ and A. To achieve complete population inversion, we must demand

$$\Delta = 0, \quad A = (2k + 1)\pi, \tag{6}$$

with an arbitrary integer k. It is the so-called resonant π pulse [101] when $k = 0$.

One can see from Eq. (5) that the resonant π pulse strictly depends on the conditions that the detuning must vanish and the pulse area must precisely be π. In practice, physical parameters often suffer from external perturbations such as inhomogeneous broadening, Doppler broadening, spatial intensity distribution, transit time variation, unwanted chirp, and shape distortions. As a result, the parameters fail to reach accurate values and thus produce errors. These errors ultimately affect the effectiveness of population inversion. Therefore, the resonant π pulse is highly sensitive to errors. To solve this problem, we can turn to the CP sequence.

Here, we study the most general situation; that is, the CP sequence consists of N single off-resonant pulses. Without loss of generality, we set the phase of the first pulse as zero, i.e., $\theta_1 = 0$, because it is the overall phase for the CP sequence, and all others are the relative phases with respect to the first pulse [29]. Under this premise, the CP sequence possesses $(3N - 1)$ free modulation parameters, i.e., $\{\Delta_n, A_n, \theta_n\}$ with $n = 1, \ldots, N$. For brevity of expression, we also integrate θ_1 into the modulation parameters hereafter. According to Eq. (4), we first write down the propagator of the nth pulse,

$$\boldsymbol{U}_n(\tau_n) = \begin{bmatrix} \cos\frac{A_n}{2} + i\frac{\Delta_n\sin\frac{A_n}{2}}{\sqrt{\Delta_n^2+1}} & -i\frac{\sin\frac{A_n}{2}}{\sqrt{\Delta_n^2+1}}e^{i\theta_n} \\ -i\frac{\sin\frac{A_n}{2}}{\sqrt{\Delta_n^2+1}}e^{-i\theta_n} & \cos\frac{A_n}{2} - i\frac{\Delta_n\sin\frac{A_n}{2}}{\sqrt{\Delta_n^2+1}} \end{bmatrix}. \tag{7}$$

Then, the total propagator of the CP sequence with N pulses is represented by

$$\begin{aligned}\boldsymbol{U}^{(N)}(T) &= \boldsymbol{U}_N(\tau_N)\boldsymbol{U}_{N-1}(\tau_{N-1})\cdots\boldsymbol{U}_1(\tau_1) \\ &= \begin{bmatrix} U_{11}^{(N)}(T) & U_{12}^{(N)}(T) \\ U_{21}^{(N)}(T) & U_{22}^{(N)}(T) \end{bmatrix},\end{aligned} \tag{8}$$

where T is the total duration, and $\tau_n = (t_n - t_{n-1})$ is the duration of the nth pulse ($t_0 = 0$ and $t_N = T$). As a result, the probability amplitude vector at the evolution time T reads

$$\boldsymbol{c}(T) = \begin{bmatrix} U_{11}^{(N)}(T) \\ U_{21}^{(N)}(T) \end{bmatrix}. \tag{9}$$

Provided that the error appears in the system, the parameters become imprecise, leading to the unfavorable influence on the propagator. As a result, the transition probability of the target state inevitably deviates from the desired value. For simplicity, we denote the generalized error as ϵ, universally referring to all kinds of parameter errors in the system. On this occasion, the total propagator of the N-pulse sequence becomes $\boldsymbol{U}_{\epsilon}^{(N)}(T)$, and the transition probability of the state $|\psi_2\rangle$ reads $P_{\epsilon}^{(N)} = |U_{\epsilon,21}^{(N)}(T)|^2$. To intuitively visualize the influence of the error on the transition probability, it is feasible to divide $P_{\epsilon}^{(N)}$ into multiple error terms by the Taylor expansion, and the expression can be written as

$$P_{\epsilon}^{(N)} = a_0 + \alpha_e(\epsilon), \tag{10}$$

where a_0 is the accurate transition probability of the state $|\psi_2\rangle$ in the absence of the error, and $\alpha_e(\epsilon)$ denotes all error terms. Specifically, $\alpha_e(\epsilon)$ has the following form:

$$\alpha_e(\epsilon) = \sum_{m=1}^{\infty} a_m \epsilon^m, \tag{11}$$

where the coefficient of the mth-order error term is

$$a_m = \frac{1}{m!} \frac{\partial^m}{\partial \epsilon^m} P_{\epsilon}^{(N)} \bigg|_{\epsilon=0}. \tag{12}$$

It is easily seen from Eq. (11) that if $\epsilon \neq 0$, $\alpha_e(\epsilon)$ is always nonzero and thus adversely influences the transition probability of the state $|\psi_2\rangle$. To achieve population transfer in a robust manner, the value of $\alpha_e(\epsilon)$ needs to be sharply suppressed. To this end, the modulation parameters $\{\Delta_n, A_n, \theta_n\}$ in the N-pulse sequence can be designed by solving the following equations:

$$\begin{cases} a_0 = \gamma, \\ a_1 = 0, \\ a_2 = 0, \\ \quad \vdots \end{cases} \tag{13}$$

where γ is the predetermined transition probability of the state $|\psi_2\rangle$.

Actually, the above idea of extracting and nullifying error terms in the Taylor expansion is popularly used for the construction of CP sequences [28,29]. Various CP sequences with different modulations have been applied to robust quantum control [88–97]. For example, a typical CP sequence with the phase modulation [28] was proposed to implement high-fidelity quantum information processing. Through the strength modulation, Wang *et al.* [92,93] exploited CPs to dramatically suppress the error caused by the Overhauser noise [102] and the charge noise [103]. Besides, the detuning-modulation CP sequence [96] showed great success in realizing complete light transfer with better insensitivity to fabrication errors in optical waveguide systems. Recently, most CP sequences have been available to test on an IBM quantum computer [104], providing a very efficient tool in quantum information processing.

Nevertheless, there are still two issues that need to be addressed during the design of CP sequences. The first one is that the effectiveness of these CPs [28–31,96–98,105–107] relies on the conditions in Eqs. (13) being completely solvable. Provided that there is no solution for Eqs. (13), complete nullification of the error terms becomes impossible. As a result, the CP sequences would fail to be constructed. Another issue is that different types of errors may simultaneously exist in the system. Then, more than one error term with the same order are contained in the Taylor series of the transition probability. On this occasion, the number of the modulation parameters may be too small to satisfy Eqs. (13), especially in the short pulse sequence. What is more, these CPs [28–31,96–98,105–107] do not focus on the optimum efficiency in terms of robustness.

Here, we put forward a cost function to tackle these issues. The cost function is made up of the error coefficients from Eq. (11), each accompanied by a weighting factor. The expression is given by

$$\mathcal{J}_{\mathcal{M}} = \sum_{m=1}^{\mathcal{M}} r^m a_m^2, \tag{14}$$

where r is a positive constant satisfying $0 < r \leqslant 1$, and the error coefficients are truncated to the $\mathcal{M}$th order. Note that the weighting factor r^m exponentially declines as the order of the error coefficients increases. The purpose of integrating the weighting factor in the cost function is found as follows. If r is much less than 1, the cost function is "shortsighted." That is, the value of the cost function primarily depends on the value of the low-order coefficients, and the contribution of high-order coefficients can be almost ignored. As r approaches 1, the cost function takes more account of the influence of high-order coefficients. When $r = 1$, the coefficients of each order make the same contribution to the cost function. Therefore, the value of r actually determines the effective contribution of high-order coefficients to the cost function. Note that the value of r is expected to be small here, because the value of the error coefficient a_m increases as the order increases.

When the cost function reaches the minimum value, the low-order coefficients are likewise suppressed to low values, resulting in the CPs being robust against the errors. Therefore, the problem of designing the optimal CPs in terms of robustness is now transformed into searching the minimum value of the cost function under the given constraint, i.e.,

$$\min_{\Delta_n, A_n, \theta_n} \mathcal{J}_{\mathcal{M}} = \sum_{m=1}^{\mathcal{M}} r^m a_m^2, \quad \text{such that } a_0 = \gamma. \tag{15}$$

The introduction of the constraint in Eq. (15) is to achieve the predetermined transition probability γ of the state $|\psi_2\rangle$.

If the errors simultaneously appear in two parameters, which are labeled as ϵ_1 and ϵ_2, the Taylor series in Eq. (11)

needs to change into

$$\alpha_e(\epsilon_1, \epsilon_2) = \sum_{m,l=0}^{\mathcal{M}} a_{m,l}\, \epsilon_1^m \epsilon_2^l, \quad m + l \neq 0, \tag{16}$$

where $a_{m,l}$ is the coefficient of the $(m + l)$th-order error term, and m and l represent the orders of errors ϵ_1 and ϵ_2, respectively. In this situation, the cost function is accordingly modified as

$$\mathcal{J}_{\mathcal{M}} = \sum_{m,l=0}^{\mathcal{M}} r^{m+l} a_{m,l}^2, \tag{17}$$

where the error coefficients with the same order have the identical weighting factor. Note that, however many types of errors there are in the system, we can design a similar form of the cost function in Eq. (17) using the same construction method. Upon finding the minimum value of the cost function, we naturally obtain the modulation parameters $\{\Delta_n, A_n, \theta_n\}$ of the CP sequence. As a result, this optimal CP sequence would be robust against multiple types of errors.

There are numerous methods to seek out the minimum value of the cost function. Among them, the Lagrangian multiplier method [75] performs well, especially in the case where the cost function is restricted by certain constraints. For instance, in terms of Eq. (15), we establish the Lagrangian function

$$\mathcal{L} = \mathcal{J}_{\mathcal{M}} + \lambda_0(a_0 - \gamma), \tag{18}$$

where the dimensionless parameter λ_0 is called the Lagrangian multiplier. Then, we have to nullify the first partial derivatives of the Lagrangian function $\mathcal{L}$ with respect to Δ_n, A_n, θ_n, and λ_0, i.e.,

$$\begin{cases} \dfrac{\partial \mathcal{L}}{\partial \Delta_1} = \cdots = \dfrac{\partial \mathcal{L}}{\partial \Delta_N} = 0, \\ \dfrac{\partial \mathcal{L}}{\partial A_1} = \cdots = \dfrac{\partial \mathcal{L}}{\partial A_N} = 0, \\ \dfrac{\partial \mathcal{L}}{\partial \theta_1} = \cdots = \dfrac{\partial \mathcal{L}}{\partial \theta_N} = 0, \\ \dfrac{\partial \mathcal{L}}{\partial \lambda_0} = 0. \end{cases} \tag{19}$$

It is worth mentioning that Eqs. (19) make up a set of algebraic equations rather than differential equations, since $\mathcal{L}$ is a well-defined elementary function and the analytical expressions for the first partial derivative of the Lagrangian function $\mathcal{L}$ are readily acquired. Furthermore, the solution of Eqs. (19) always exists because the cost function $\mathcal{J}_{\mathcal{M}}$ is continuous and nonmonotonic. At this point, we solve the situation in which Eqs. (13) have no solution.

Note that the solution of Eqs. (19) may or may not be the minimum value of the cost function. Satisfying Eqs. (19) is only a necessary condition for the cost function $\mathcal{J}_{\mathcal{M}}$ to reach its minimum, but not a sufficient one. In other words, each solution of Eqs. (19) merely corresponds to an extremum value of the cost function $\mathcal{J}_{\mathcal{M}}$. Therefore, we need to acquire all solutions of Eqs. (19), and then pick up the minimum one to regard as the optimal solution. A feasible way of doing this is to repetitively solve Eqs. (19) with large amounts of random initial parameters, because different initial parameters may converge to a different solution in numerical calculations. When the initial parameters are selected enough times, in principle, we would make a traversal over all extremum values of the cost function. As a result, the optimal modulation parameters corresponding to the minimum value of the cost function can be readily sought out. To make it more intuitive, we present the detailed workflow for searching the optimal modulation parameters in Algorithm 1.

Algorithm 1. Pseudocode of searching the optimal modulation parameters of CPs.

Initialize:

(1) Randomly select a set of initial parameters $\mathcal{I}_k' = \{\Delta_n'^k, A_n'^k, \theta_n'^k, \lambda_0'^k\}$ and solve Eqs. (19);

(2) The solutions are denoted as $\mathcal{I}_{\text{opt}} = \{\Delta_n^{\text{opt}}, A_n^{\text{opt}}, \theta_n^{\text{opt}}, \lambda_0^{\text{opt}}\}$ and the corresponding cost function is denoted as $\mathcal{J}_{\min}$;

(3) The index of iterations $k = 1$.

Repeat: (for each iterative process)

(4) Go to step 1;

(5) Obtain the solution $\mathcal{I}_k = \{\Delta_n^k, A_n^k, \theta_n^k, \lambda_0^k\}$ and the corresponding cost function $\mathcal{J}_{\mathcal{M},k}$;

(6) **If:** $\mathcal{J}_{\min} > \mathcal{J}_{\mathcal{M},k}$;

Then: $\mathcal{J}_{\min} \leftarrow \mathcal{J}_{\mathcal{M},k}$, $\mathcal{I}_{\text{opt}} \leftarrow \mathcal{I}_k$;

Until: Reach the maximum iteration $k = K_{\max}$;

Output: The optimal parameters $\mathcal{I}_{\text{opt}} = \{\Delta_n^{\text{opt}}, A_n^{\text{opt}}, \theta_n^{\text{opt}}, \lambda_0^{\text{opt}}\}$ and the minimum cost function $\mathcal{J}_{\min}$.

So far, we have constructed the optimal CPs in terms of robustness by searching the minimum value of the cost function. In this case, the low-order coefficients are usually nonzero, although they may be extremely small. As demonstrated in Eq. (11), the low-order coefficients have a larger impact on the transition probability than the high-order ones. Therefore, the implementation of population transfer with ultrahigh fidelity cannot be guaranteed, provided that the low-order coefficients do not vanish. In fact, this flaw can be overcome by introducing additional constraints on the cost function $\mathcal{J}_{\mathcal{M}}$. The additional constraints are

$$a_1 = a_2 = \cdots = a_M = 0, \tag{20}$$

where the subscript M is the highest order of error terms to be nullified. Alternatively, we can treat the solvable equations in Eqs. (13) as additional constraints and discard those that are unsolvable. As a result, the cost function $\mathcal{J}_{\mathcal{M}}$ in Eq. (14) becomes

$$\mathcal{J}_{\mathcal{M}} = \sum_{m=M+1}^{\mathcal{M}} r^m a_m^2. \tag{21}$$

Then, the optimal control problem in Eq. (15) is changed to

$$\min_{\Delta_n, A_n, \theta_n} \mathcal{J}_{\mathcal{M}} = \sum_{m=M+1}^{\mathcal{M}} r^m a_m^2, \tag{22}$$

$$\text{such that } a_0 = \gamma,\ a_1 = \cdots = a_M = 0.$$

In this situation, the Lagrangian function becomes

$$\mathcal{L}' = \mathcal{J}_{\mathcal{M}} + \lambda_0(a_0 - \gamma) + \sum_{m=1}^{M} \lambda_m a_m. \tag{23}$$

Similar to Eqs. (19), the extreme values of the cost function are attained by solving the following equations:

$$\begin{cases} \dfrac{\partial \mathcal{L}'}{\partial \Delta_1} = \cdots = \dfrac{\partial \mathcal{L}'}{\partial \Delta_N} = 0, \\ \dfrac{\partial \mathcal{L}'}{\partial A_1} = \cdots = \dfrac{\partial \mathcal{L}'}{\partial A_N} = 0, \\ \dfrac{\partial \mathcal{L}'}{\partial \theta_1} = \cdots = \dfrac{\partial \mathcal{L}'}{\partial \theta_N} = 0, \\ \dfrac{\partial \mathcal{L}'}{\partial \lambda_0} = \cdots = \dfrac{\partial \mathcal{L}'}{\partial \lambda_M} = 0. \end{cases} \tag{24}$$

Through employing Algorithm 1 once again, we would acquire all modulation parameters of the optimal CP sequence. Note that this CP sequence does have excellent performance in the ultrahigh-excitation region of the transition probability, due to complete nullification of the low-order coefficients.

III. CONFIGURATION OF THE COST FUNCTION

The specific form of the cost function $\mathcal{J}_{\mathcal{M}}$ in Eq. (14) is associated with two configuration parameters, the weighting factor r and the truncated highest order $\mathcal{M}$. Different r and $\mathcal{M}$ may cause the modulation parameters $\{\Delta_n, A_n, \theta_n\}$ to be different, resulting in various performances of the obtained optimal CPs. Therefore, it is significant to investigate the range of r and $\mathcal{M}$ in the cost function $\mathcal{J}_{\mathcal{M}}$. In the following, we utilize the two-pulse sequence to exemplify this issue.

Provided that the error appears in the pulse area, the actual area of the nth pulse becomes $A_n \to A_n(1+\epsilon_A)$. Then, the form of the propagator of the two-pulse sequence reads

$$\boldsymbol{U}^{(2)}_{\epsilon_A}(T,0) = \boldsymbol{U}_2(\tau_2)\boldsymbol{U}_1(\tau_1). \tag{25}$$

By the Taylor expansion, we rearrange the transition probability of the state $|\psi_2\rangle$ into different error terms,

$$P^{(2)}_{\epsilon_A} = a_0 + \sum_{m=1}^{\infty} a_m \epsilon_A^m. \tag{26}$$

As a result, the corresponding cost function is designed as

$$\mathcal{J}_{\mathcal{M}} = \sum_{m=1}^{\mathcal{M}} r^m a_m^2. \tag{27}$$

To estimate the robust performance of different CP sequences, we quantify the width W_k $(k = 0, 1, 2, \ldots)$ of the high-excitation range, and its definition is given by

$$W_k = \tfrac{1}{2}(\epsilon^+_{A,k} - \epsilon^-_{A,k}), \tag{28}$$

where $\epsilon^+_{A,k}$ and $\epsilon^-_{A,k}$ are two solutions to the following equation:

$$P^{(2)}_{\epsilon_A} = 1 - 10^{-k}. \tag{29}$$

Namely, we have $P^{(2)}_{\epsilon_A} \geqslant 1 - 10^{-k}$, if $\epsilon_A \in [\epsilon^-_{A,k}, \epsilon^+_{A,k}]$.

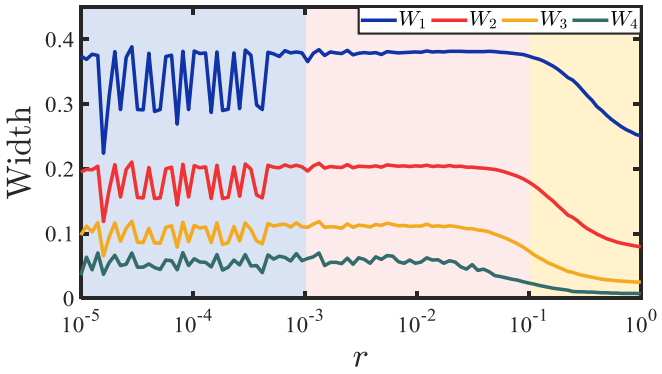

FIG. 1. The width W_k of the high-excitation range vs the weighting factor r, where the modulation parameters of the optimal CP sequences are obtained by minimizing the cost function $\mathcal{J}_5$.

Figure 1 demonstrates the width W_k as a function of the weighting factor r, where different values of r correspond to different cost functions. By minimizing these cost functions, one can obtain various modulation parameters and thus design different optimized sequences. It can be seen that when r is large (e.g., $r \in [10^{-1}, 1]$ in Fig. 1), the width W_k is relatively narrow and increases as r decreases. The reason is that a large r makes high-order coefficients contribute more to the cost function given by Eq. (27). In this case, the low-order coefficients cannot be diminished preferentially, so the robust performance of CPs is not particularly excellent. When $r \in [10^{-3}, 10^{-1}]$, the width W_k becomes steady and keeps a high value, since the contribution of more low-order coefficients is considered in the cost function. We can also find that the r suitable for the optimal pulse design is not a specific value, but a range. Finally, when r is overly small, e.g., $r < 10^{-3}$, the width W_k begins to oscillate. Specifically, the oscillations become more and more pronounced as r further decreases. This is because the low-order coefficients contribute overmuch in the cost function. In other words, the cost function is very "shortsighted." Hence, for an overly small r, we may not obtain the modulation parameters of CPs for the optimal robustness against errors.

To understand more about the reason for the oscillation phenomenon in Fig. 1, by taking $r = 0.0001$, we plot in Fig. 2 the excitation profiles for different sets of CP sequences obtained through different extreme values of the cost function $\mathcal{J}_5$, where the relevant parameters are given in Table I. It is clear from Table I that the $\mathrm{E2}^{[1]}_{\epsilon_A}$ sequence is the optimal one since the corresponding cost function is minimal, but its robust performance in Fig. 2 is not the best. The root cause of this result is that a small r can reduce the contribution of high-order coefficients, but an overly small one may produce the counterproductive effect. To be specific, the smaller r is, the smaller the contribution of high-order coefficients will be. Under the limit $r \to 0$, the cost function in Eq. (27) is only dominated by the first-order coefficient a_1. As presented in Table I, when $r = 0.0001$, the first three order coefficients a_1, a_2, and a_3 make the major contributions to the value of the cost function $\mathcal{J}_5$, while the fourth-order coefficient a_4 does not affect $\mathcal{J}_5$ very much. Namely, although $\mathcal{J}_5$ is minimal in the $\mathrm{E2}^{[1]}_{\epsilon_A}$ sequence, the coefficient a_4 is much larger than those in the other three sequences, leading to a narrower

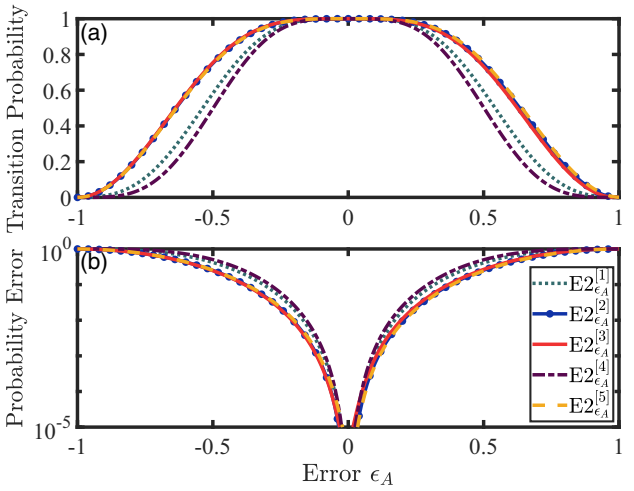

FIG. 2. (a) Excitation profiles for the $E2^{[l]}_{\epsilon_A}$ sequence ($l = 1, \ldots, 5$), where $r = 0.0001$ and the modulation parameters come from Table I. The $E2^{[1]}_{\epsilon_A}$ sequence is the optimal one, while the other sequences are obtained by the extreme values of the cost function $\mathcal{J}_5$. (b) Transition probability error $1 - P^{(2)}_{\epsilon_A}$ vs the pulse area error ϵ_A in a logarithmic scale.

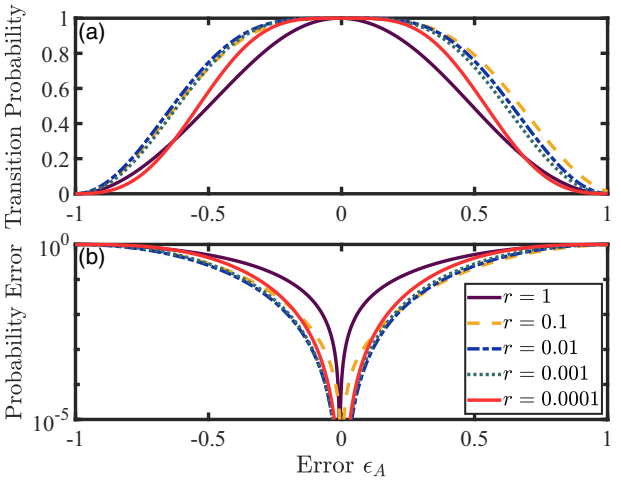

FIG. 3. (a) Excitation profiles for different optimal CPs by choosing $r = 10^{-k}$ in the cost function $\mathcal{J}_4$, where $k = 0, \ldots, 4$. (b) Transition probability error $1 - P^{(2)}_{\epsilon_A}$ vs the error ϵ_A in a logarithmic scale.

high-excitation range in Fig. 2. Therefore, a moderately small magnitude of the weighting factor in the cost function is the wise choice for constructing the optimal CP sequence.

Next, we plot in Fig. 3 the excitation profiles using several special values of r to further demonstrate the validity of the cost function. As shown by the purple solid curve, the transition probability suffers seriously from the tiny error, and drops rapidly as the error increases. This means that when all error coefficients a_m are considered with the same contribution ($r = 1$), the solution (i.e., the modulation parameters of the optimal CP sequence) that minimizes the cost function $\mathcal{J}_4$ is not suitable for constructing CPs that are robust against the errors. Likewise, for the overly small r, e.g., $r = 0.0001$, the matched CPs cannot achieve optimal error compensation (see the solid red curve). Therefore, Fig. 3 again verifies that the value of r should be appropriately small in order to obtain the optimal robustness with respect to the errors. From the perspectives of the stability and wide excitation profile, we choose $r = 0.01$ hereafter.

Figure 4 shows the robust performances of different optimal CPs by choosing different $\mathcal{M}$ in the cost function $\mathcal{J}_\mathcal{M}$, where the modulation parameters are obtained through Algorithm 1. An inspection of Fig. 4 demonstrates that the robustness against the error becomes much stronger with the increase of $\mathcal{M}$. When $\mathcal{M}$ exceeds a certain value (e.g., $\mathcal{M} \geqslant 4$ in the two-pulse sequence), the robustness hardly changes, as shown by the solid blue, solid orange, and dashed pink curves in Fig. 4. In other words, the solution of the minimum cost function, i.e., the modulation parameters of the optimal CP sequence, keeps unchanged when $\mathcal{M}$ is sufficiently large. The reason for these results can be found as follows.

As indicated in Sec. II, in the N-pulse sequence, only $(3N - 2)$ modulation parameters are available to reduce the impact of errors on the transition probability, because one of them must be used for satisfying the constraint $a_0 = \gamma$. When $\mathcal{M}$ is larger than $(3N - 2)$, cf. $\mathcal{M} = 5$ or 6 in the two-pulse sequence, the robustness will not be much improved. This implies that the contribution of high-order coefficients can be ignored in the cost function. On the other hand, when $\mathcal{M} \ll (3N - 2)$, cf. $\mathcal{M} = 1$ or 2 in the two-pulse sequence, the free modulation parameters are surplus. In this situation, although the minimum value of the cost function can reach zero, the coefficients above the $(\mathcal{M} + 1)$th order are not involved in the cost function. As a result, the robust performance is not particularly good; see the solid purple and red curves in Fig. 4. Therefore, in the N-pulse sequence, the highest order of the cost function is at least truncated to $(3N - 2)$, i.e., $\mathcal{M} \geqslant 3N - 2$.

TABLE I. Numerical results for different CP sequences obtained by five sets of extremal solutions to Eq. (19), where we set $r = 0.0001$.

	Cost function		Error coefficients					Modulation parameters				
Sequence	$\mathcal{J}_5$	a_0	a_1	a_2	a_3	a_4	a_5	Δ_1/Ω_1	Δ_2/Ω_2	A_1	A_2	θ_2
$E2^{[1]}_{\epsilon_A}$	3.6006×10^{-14}	1	1.0895×10^{-6}	0.0001	0.1347	−13.2992	−0.5626	−1.7312	0.0287	5.7524	2.8836	3.5918
$E2^{[2]}_{\epsilon_A}$	3.9485×10^{-14}	1	1.9030×10^{-6}	−0.0019	−0.0286	−6.1353	0.0708	−1.0817	0.9151	3.2982	3.0047	−0.2083
$E2^{[3]}_{\epsilon_A}$	2.5835×10^{-13}	1	3.8698×10^{-5}	−0.0028	−0.1634	−6.2521	0.4091	−1.0510	0.9458	3.2784	3.0520	6.1247
$E2^{[4]}_{\epsilon_A}$	2.3993×10^{-13}	1	-3.6801×10^{-5}	0.0024	0.1091	−18.2410	−0.5383	0.0014	1.9127	3.1426	6.2853	3.2520
$E2^{[5]}_{\epsilon_A}$	2.7094×10^{-12}	1	1.4681×10^{-4}	−0.0074	0.0901	−5.9831	−0.2215	−0.9700	1.0245	3.0087	3.2542	0.1761

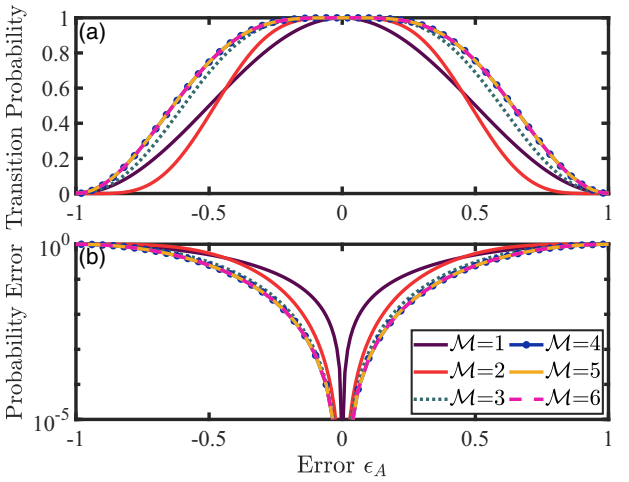

FIG. 4. (a) Excitation profiles for different optimal CPs by choosing $\mathcal{M} = 1, \ldots, 6$ in the cost function $\mathcal{J}_{\mathcal{M}}$, where $r = 0.01$. (b) Transition probability error $1 - P^{(2)}_{\epsilon_A}$ vs the error ϵ_A in a logarithmic scale.

IV. OPTIMAL ROBUST PULSE DESIGN

In this section, we illustrate the detailed CP design for optimizing the robustness with respect to different errors.

First, we explain several typical types of errors that commonly appear during quantum operations. One of them is the pulse duration error. A direct source for this error is the imprecise duration of the CP sequence, which may be caused by manual manipulation faults or experimental defects. Unfortunately, we cannot prevent the occurrence of this error in some cases. For example, when a beam of atoms passes through a laser field, due to the nonuniformity of the atomic longitudinal velocity [11], the interaction time between each atom and the laser field is usually different. In order to quantify the error caused by the pulse duration, we introduce a small unknown constant ϵ_τ, and write the actual duration as

$$\tau_n \to \tau_n(1 + \epsilon_\tau). \tag{30}$$

In fact, the pulse duration error is also equivalent to the pulse area error, which can be seen from the following relation:

$$A_n(1 + \epsilon_A) = \Omega_n \sqrt{\chi_n^2 + 1}\, \tau_n(1 + \epsilon_\tau). \tag{31}$$

Therefore, we substitute the pulse area error ϵ_A for the pulse duration error ϵ_τ in the following.

Another significant one is the coupling strength error. Here, we employ ϵ_Ω to represent this error, and the actual coupling strength becomes

$$\Omega_n \to \Omega_n(1 + \epsilon_\Omega). \tag{32}$$

This type of error is often induced by the inhomogeneity of control fields. In the singlet-triplet spin qubit, it originates from the fluctuations of the magnetic field gradient [92,93], while it comes from the uneven spatial distribution of laser fields in the atom-laser system. Moreover, the atoms always slightly oscillate at their equilibrium position, leading to the generation of the coupling strength error as well.

The third type is the detuning error, produced by the energy-level shift or the control field frequency drift. One representative phenomenon is the Stark shift [101], where the energy level shifts slightly on account of the interaction with external fields. In doped crystals [30,98,108], the transition frequency of different ions would be distinct due to the widened hyperfine levels. To study the impact of the detuning error on the transition probability, we add an unknown constant ϵ_Δ to the original detuning,

$$\Delta_n \to \Delta_n + \epsilon_\Delta.$$

Next, we expand this issue in terms of the single error and multiple errors, respectively.

A. Single error

1. Population inversion

In this section, we first study how to implement complete population inversion by setting $N = 2$, and label the single error as ϵ, which represents one of three errors, i.e., ϵ_A, ϵ_Ω, or ϵ_Δ. For simplicity of expression, the optimal N-pulse sequence compensating for the single error ϵ is termed as the $\mathrm{O}N_\epsilon$ sequence henceforth. In the presence of the single error ϵ, the Taylor series of the transition probability of the state $|\psi_2\rangle$ is given by

$$P^{(2)}_\epsilon = a_0 + \sum_{m=1}^{\infty} a_m \epsilon^m, \tag{33}$$

where the zero-order coefficient reads

$$\begin{aligned} a_0 = \frac{1}{(1+\Delta_1^2)(1+\Delta_2^2)}\Bigg[& \sin^2\frac{A_1}{2}\cos^2\frac{A_2}{2} + \cos^2\frac{A_1}{2}\sin^2\frac{A_2}{2} + \Delta_1^2\sin^2\frac{A_2}{2} + \Delta_2^2\sin^2\frac{A_1}{2} \\ & + 2\sin\frac{A_1}{2}\sin\frac{A_2}{2}\sin\theta_2\left(\Delta_1\sqrt{1+\Delta_2^2}\sin\frac{A_1}{2}\cos\frac{A_2}{2} + \Delta_2\sqrt{1+\Delta_1^2}\cos\frac{A_1}{2}\sin\frac{A_2}{2}\right) \\ & + 2\sin\frac{A_1}{2}\sin\frac{A_2}{2}\cos\theta_2\left(\sqrt{1+\Delta_1^2}\sqrt{1+\Delta_2^2}\cos\frac{A_1}{2}\cos\frac{A_2}{2} - \Delta_1\Delta_2\sin\frac{A_1}{2}\sin\frac{A_2}{2}\right)\Bigg]. \end{aligned} \tag{34}$$

There are five free modulation parameters in the $\mathrm{O}2_\epsilon$ sequence, i.e., $\{\Delta_1, \Delta_2, A_1, A_2, \theta_2\}$. To maximize the robustness of the system against errors, one parameter is required to make the inerrant transition probability (i.e., the zero-order coefficient a_0) equal to one, while the other four parameters are aimed at completely canceling the first fourth-order

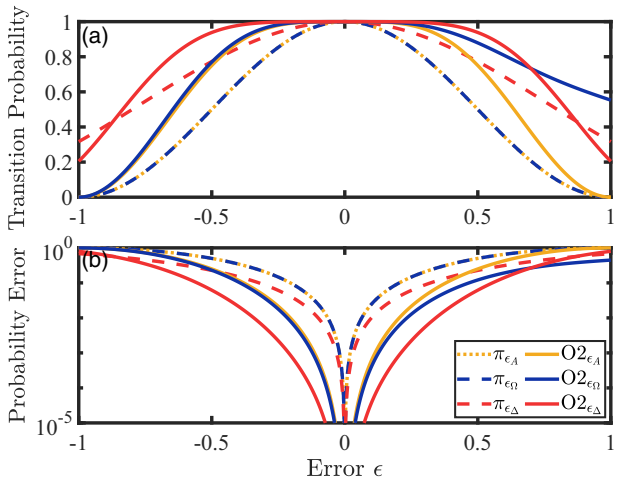

FIG. 5. (a) Excitation profiles for the single resonant π pulse (π_{ϵ_A}, π_{ϵ_Ω}, and π_{ϵ_Δ}) and the two-pulse sequence ($O2_{\epsilon_A}$, $O2_{\epsilon_\Omega}$, and $O2_{\epsilon_\Delta}$), where the modulation parameters come from Table II. (b) Transition probability error $1 - P_\epsilon^{(2)}$ vs the error ϵ in a logarithmic scale.

coefficients in Eq. (10). As a result, the five equations to be solved read

$$\begin{cases} a_0 = 1, & \text{(35a)} \\ a_1 = 0, & \text{(35b)} \\ a_2 = 0, & \text{(35c)} \\ a_3 = 0, & \text{(35d)} \\ a_4 = 0. & \text{(35e)} \end{cases}$$

Unfortunately, there is no feasible solution for these equations. This problem can be well settled by regarding Eqs. (35a)–(35d) as the constraints of the cost function given by Eq. (21). Therefore, the current task becomes

$$\min_{\Delta_n, A_n, \theta_n} \mathcal{J}_6 = r^4 a_4^2 + r^5 a_5^2 + r^6 a_6^2,$$
$$\text{such that } a_0 = 1,\ a_1 = a_2 = a_3 = 0, \qquad (36)$$

where the coefficients of the cost function are truncated to sixth order, i.e., $\mathcal{M} = 6$.

Utilizing Algorithm 1, we numerically seek out the optimal parameters of the $O2_\epsilon$ sequence, which are presented in Table II. The corresponding excitation profiles are plotted in Fig. 5. To make a distinct comparison to the single pulse, we also exhibit the excitation profiles for the single resonant π pulse, labeled as π_{ϵ_A}, π_{ϵ_Ω}, and π_{ϵ_Δ}, respectively. Figure 5 demonstrates that the obtained $O2_\epsilon$ sequences outperform the single resonant pulse at the robustness with respect to the errors, reflected in the broader flat top of their excitation profiles. For the $O2_{\epsilon_\Delta}$ sequence, it can successfully achieve complete population inversion with ultrahigh fidelity as well even when a small detuning error appears. It is worth mentioning that the numerical solution of the $O2_{\epsilon_A}$ sequence is the same as the analytical one in Ref. [96].

TABLE II. Modulation parameters of the two-pulse sequence for complete population inversion.

Sequence	Δ_1/Ω_1	Δ_2/Ω_2	A_1	A_2	θ_2
$O2_{\epsilon_A}$	1	−1	3.1416	3.1416	0
$O2_{\epsilon_\Omega}$	0.7515	0.0003	6.2663	3.1284	3.1416
$O2_{\epsilon_\Delta}$	0.4722	−0.4722	4.4884	4.4859	0.0010
$O2^{[1]}_{\epsilon_\Delta \epsilon_A}$	0	0	4.7124	1.5708	3.1416
$O2^{[2]}_{\epsilon_\Delta \epsilon_A}$	1	−1	3.1415	3.1416	0

TABLE III. Modulation parameters of the two-pulse sequence for arbitrary population transfer.

γ	Δ_1/Ω_1	Δ_2/Ω_2	A_1	A_2	θ_2
0.1	2.1200	−3.5145	3.7681	5.1302	1.7179
0.2	3.9066	−1.8003	5.5580	3.4871	5.2689
0.3	4.2940	−1.5098	6.0143	3.2509	5.9298
0.4	4.7312	−1.2098	6.5928	3.0425	0.3798
0.5	5.2841	−0.8713	7.4985	2.9021	1.3785
0.6	−6.1200	0.5922	9.9876	3.2388	2.6193
0.7	7.4146	−0.6304	11.837	3.2387	5.5245
0.8	9.4021	−0.4284	14.199	3.0210	1.7056
0.9	1.4262	−0.1639	2.1747	3.6409	5.3246
1	1	−1	3.1416	3.1416	0

2. *Arbitrary population transfer*

The current optimal approach can also be extended for arbitrary population transfer via slightly changing the constraints of the cost function. In the following, we give a detailed description of it.

Assuming that the system exhibits the pulse area error ϵ_A, on this occasion, the first equation in Eq. (13) changes into $a_0 = \gamma$, and then the optimal problem becomes

$$\min_{\Delta_n, A_n, \theta_n} \mathcal{J}_6 = r^4 a_4^2 + r^5 a_5^2 + r^6 a_6^2,$$
$$\text{such that } a_0 = \gamma,\ a_1 = a_2 = a_3 = 0, \qquad (37)$$

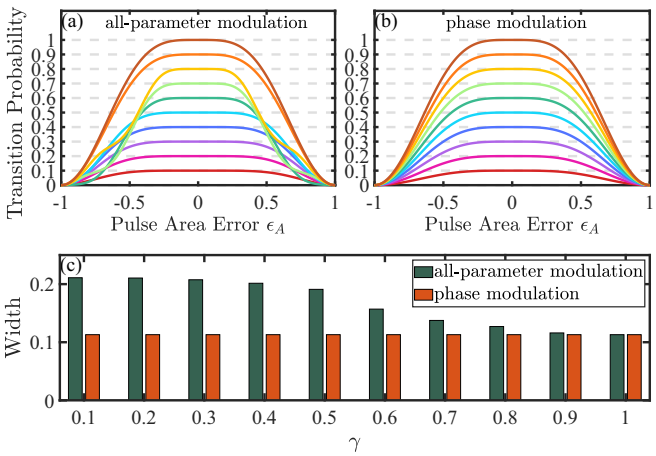

FIG. 6. Excitation profiles for the two-pulse sequence by (a) all-parameter modulation and (b) phase modulation, where the modulation parameters are given in Table III. The curves represent the transition probability γ locked at the level 0.1, 0.2, ..., and 1. (c) The high-excitation range (i.e., $P^{(2)}_{\epsilon_A} \geqslant 0.999\gamma$) for the two types of modulation.

where γ is the transition probability of the state $|\psi_2\rangle$. Similarly, we can search the optimal parameters $\{\Delta_1, \Delta_2, A_1, A_2, \theta_2\}$ of the CP sequence for different population transfer through Algorithm 1, and the numerical solutions are presented in Table III. The corresponding excitation profiles are plotted in Fig. 6(a), which shows that arbitrary population transfer is indeed achieved in a robust way.

It is easily found from Table III that all modulation parameters are different when implementing different population transfer. Even though every parameter is feasible to be adjusted, modulating all of them may increase the complexity of practical operations. An intuitive way of simplifying it is to employ a single modulation parameter (e.g., the phase θ_2), while the remaining parameters keep unchanged. To this end, we first set the pulse area of two pulses $A_1 = A_2 = \pi$. Then, the expressions of the first five coefficients in Eq. (33) are written as

$$a_0 = \frac{\Delta_1^2 + \Delta_2^2 - 2\Delta_1\Delta_2\cos\theta_2}{(\Delta_1^2+1)(\Delta_2^2+1)}, \tag{38a}$$

$$a_1 = -\pi\frac{\left(\Delta_2\sqrt{\Delta_1^2+1} + \Delta_1\sqrt{\Delta_2^2+1}\right)\sin\theta_2}{(\Delta_1^2+1)(\Delta_2^2+1)}, \tag{38b}$$

$$a_2 = -\frac{\pi^2}{4}\frac{\Delta_2^2 + (\Delta_1^2-2) - 2\left(2\Delta_1\Delta_2 + \sqrt{\Delta_1^2+1}\sqrt{\Delta_2^2+1}\right)\cos\theta_2}{(\Delta_1^2+1)(\Delta_2^2+1)}, \tag{38c}$$

$$a_3 = \frac{5\pi^3}{12}\frac{\left(\Delta_2\sqrt{\Delta_1^2+1} + \Delta_1\sqrt{\Delta_2^2+1}\right)\sin\theta_2}{(\Delta_1^2+1)(\Delta_2^2+1)}, \tag{38d}$$

$$a_4 = \frac{\pi^4}{48}\frac{\Delta_2^2 + (\Delta_1^2-8) - 2\left(5\Delta_1\Delta_2 + 4\sqrt{\Delta_1^2+1}\sqrt{\Delta_2^2+1}\right)\cos\theta_2}{(\Delta_1^2+1)(\Delta_2^2+1)}. \tag{38e}$$

We need to put the zero-order coefficient aside and preferentially cancel the first-order coefficient in Eq. (38b). For this purpose, it demands

$$\Delta_2\sqrt{\Delta_1^2+1} + \Delta_1\sqrt{\Delta_2^2+1} = 0, \tag{39}$$

since θ_2 is variable now. The solution of Eq. (39) reads

$$\Delta_2 = -\Delta_1, \tag{40}$$

which means that the detunings are antisymmetric in two pulses. Note that the coefficient a_3 is automatically nullified as well because a_1 and a_3 have the same factor. Next, we substitute the detuning relation given by Eq. (40) into Eq. (38c) to further simplify the second-order coefficient, and the corresponding equation, $a_2 = 0$, becomes

$$-\frac{\pi^2}{2}\frac{(\Delta_1^2-1)(1+\cos\theta_2)}{(\Delta_1^2+1)^2} = 0. \tag{41}$$

The solution of Eq. (41) is

$$\Delta_1 = \pm 1. \tag{42}$$

Therefore, provided that the detunings of two pulses satisfy Eqs. (40) and (42), the error coefficients up to third order are completely nullified. On this occasion, the zero- and fourth-order coefficients read

$$a_0 = \cos^2\frac{\theta_2}{2} = \gamma, \tag{43a}$$

$$a_4 = -\frac{\pi^4}{32}(1+\cos\theta_2) = -\frac{\pi^4}{16}\gamma. \tag{43b}$$

From Eqs. (43a) and (43b), we can see that the zero-order coefficient a_0 only depends on the phase θ_2, and the fourth-order coefficient a_4 cannot be nullified because it shares the same factor γ with a_0. As a result, the transition probability of the state $|\psi_2\rangle$ reads

$$P_{\epsilon_A}^{(2)} = \cos^2\frac{\theta_2}{2}\left(1 - \sin^4\frac{\pi\epsilon_A}{2}\right) = \gamma\left[1 - \frac{\pi^4}{16}\epsilon_A^4 + O(\epsilon_A^5)\right], \tag{44}$$

which is accurate to fourth order. In Fig. 6(b), we plot the excitation profiles for arbitrary population transfer by only adjusting θ_2. Remarkably, this sequence is also robust against the pulse area error.

To see the robust performance of these two CP sequences more clearly, we plot in Fig. 6(c) the high-excitation range ($P_{\epsilon_A}^{(2)} \geqslant 0.999\gamma$) of both excitation profiles. It is obvious that the optimal CP sequence by the all-parameter modulation possesses a wider high-excitation range than the sequence by merely modulating the phase θ_2. The occurrence of this phenomenon is owing to the fact that the optimized parameters can effectively reduce multiple low-order error coefficients. On the other side, as the transition probability increases, the robust advantage of the all-parameter modulation approach gradually loses, especially at high transition probabilities. Therefore, if allowing a slight sacrifice in robustness for achieving high transition probabilities, we can adopt the phase modulation approach instead, because only one parameter, rather than five parameters, needs to be adjusted.

TABLE IV. Different forms of the fourth constraint for different CP sequences.

Sequence	Fourth constraint	Eliminated error term
$O2^{[1]}_{\epsilon_\Delta\epsilon_A}$	$a_{2,0}=0$	$O(\epsilon_\Delta^2)$
$O2^{[2]}_{\epsilon_\Delta\epsilon_A}$	$a_{0,2}=0$	$O(\epsilon_A^2)$
$O2^{[2]}_{\epsilon_\Delta\epsilon_A}$	$a_{1,1}=0$	$O(\epsilon_\Delta\epsilon_A)$
$O2^{[2]}_{\epsilon_\Delta\epsilon_A}$		

B. Multiple errors

We further study the case of multiple types of errors. Provided that the system exhibits the detuning error ϵ_Δ and the pulse area error ϵ_A at the same time, then we label the transition probability of the state $|\psi_2\rangle$ as $P^{(2)}_{\epsilon_\Delta\epsilon_A}$. The Taylor series at $\epsilon_\Delta=0$ and $\epsilon_A=0$ reads

$$P^{(2)}_{\epsilon_\Delta\epsilon_A}=a_0+a_{1,0}\epsilon_\Delta+a_{0,1}\epsilon_A+a_{2,0}\epsilon_\Delta^2+a_{1,1}\epsilon_\Delta\epsilon_A+a_{0,2}\epsilon_A^2+O\big(\epsilon_\Delta^3,\epsilon_\Delta^2\epsilon_A,\epsilon_\Delta\epsilon_A^2,\epsilon_A^3\big). \tag{45}$$

It is clear that there are six error coefficients $\{a_0,a_{1,0},a_{0,1},a_{2,0},a_{1,1},a_{0,2}\}$ up to second order. Generally speaking, five free modulation parameters cannot be used to completely nullify all second-order coefficients in Eq. (45). Hence, we turn to minimize the cost function to obtain the modulation parameters of CPs, where the first-order and partial second-order coefficients are regarded as the constraints of the cost function. To be specific, the first three constraints are served for obtaining the maximum transition probability of the state $|\psi_2\rangle$ and nullifying the first-order coefficients. As a result, the cost function can be of the following form:

$$\mathcal{J}_2=r^2\big(a_{2,0}^2+a_{1,1}^2+a_{0,2}^2\big) \tag{46}$$

with the first three constraints

$$a_0=1,\quad a_{1,0}=a_{0,1}=0. \tag{47}$$

Notice that nullifying different second-order coefficients results in different robust performances of the CP sequences. In Table IV, we present different forms of the fourth constraint to implement different CP sequences.

The $O2^{[1]}_{\epsilon_\Delta\epsilon_A}$ sequence is designed for strong robustness against the detuning error. In this case, the second-order error term ϵ_Δ^2 needs to be nullified; i.e., the fourth constraint is $a_{2,0}=0$. The optimal solution is given in Table III, and the excitation profile for this sequence is depicted in Fig. 7(a). As expected, this sequence is remarkably robust against the detuning error around $\epsilon_A=0$; see the transverse region surrounded by the solid green curve in Fig. 7(a).

Similarly, the $O2^{[2]}_{\epsilon_\Delta\epsilon_A}$ sequence is built to better compensate for the pulse area error. Thus, we require to nullify the term ϵ_A^2, and the fourth constraint in the cost function becomes $a_{0,2}=0$. We display the excitation profile with respect to the errors ϵ_Δ and ϵ_A in Fig. 7(b). Clearly, due to the disappearance of the error term $O(\epsilon_A^2)$, the $O2^{[2]}_{\epsilon_\Delta\epsilon_A}$ sequence predominantly improves robustness against the pulse area error around $\epsilon_\Delta=0$, as shown in the longitudinal region enclosed by the solid green curve in Fig. 7(b).

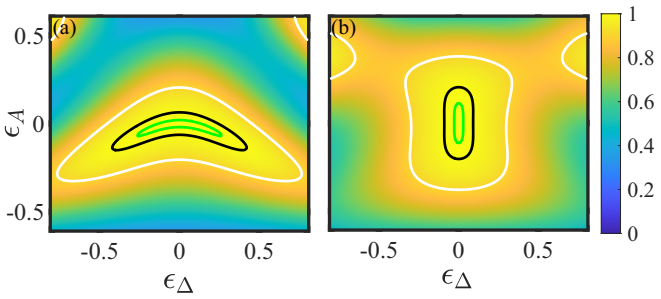

FIG. 7. Transition probability $P^{(2)}_{\epsilon_\Delta\epsilon_A}$ vs the errors ϵ_Δ and ϵ_A in (a) the $O2^{[1]}_{\epsilon_\Delta\epsilon_A}$ sequence and (b) the $O2^{[2]}_{\epsilon_\Delta\epsilon_A}$ sequence, where the modulation parameters are given in Table II. The white, black, and green curves correspond to $P^{(2)}_{\epsilon_\Delta\epsilon_A}=0.9$, 0.99, and 0.999, respectively (from outside in).

If aiming at compensating for both errors, one feasible way is to nullify the term $\epsilon_\Delta\epsilon_A$ in the Taylor series (45). At this point, the fourth constraint comes into $a_{1,1}=0$. Another alternative way is to leave out the fourth constraint. Then, we employ the remaining two modulation parameters to directly minimize the cost function. Coincidentally, we find that the modulation parameters by both approaches are the same as that of the $O2^{[2]}_{\epsilon_\Delta\epsilon_A}$ sequence. Therefore, their excitation profiles are also the same as in Fig. 7(b).

Actually, the above method of minimizing the cost function to implement robustness against the errors ϵ_Δ and ϵ_A can be readily extended to other types of errors, such as the detuning error ϵ_Δ and the Rabi frequency error ϵ_Ω. Through doing a Taylor expansion of the transition probability at $\epsilon_\Delta=0$ and $\epsilon_\Omega=0$ and then constructing the corresponding cost function, we would obtain the optimized sequences in a similar way.

V. COMPARISON WITH OTHER COMPOSITE PULSES

In this section, we make a comparison of the acquired optimal CPs with other sequences in terms of robustness. Previous CP schemes [96–98] mainly use a certain type of modulation parameters, whereas we modulate all of them in the current optimized sequences. Here, we take the pulse number $N=3$ as an example to demonstrate the robust contrast achieved by the current approach and the previous ones. In the case of the single error, we quantify the high-excitation range to assess the robustness of different CPs against the pulse area error. When considering the detuning error and the pulse area error, we measure the high-excitation region to estimate the robust performance of different CPs.

A. Single error

In the presence of the pulse area error, the propagator of the three-pulse sequence is given by

$$\boldsymbol{U}^{(3)}_{\epsilon_A}(T,0)=\boldsymbol{U}_3(\tau_3)\boldsymbol{U}_2(\tau_2)\boldsymbol{U}_1(\tau_1). \tag{48}$$

By the Taylor expansion, the transition probability of the state $|\psi_2\rangle$ reads

$$P^{(3)}_{\epsilon_A}=a_0+\sum_{m=1}^{\infty}a_m\epsilon_A^m. \tag{49}$$

TABLE V. Modulation parameters of different CP sequences for complete population inversion.

Sequence	Δ_1/Ω_1	Δ_2/Ω_2	Δ_3/Ω_3	A_1	A_2	A_3	θ_2	θ_3
$O3_{\epsilon_A}$	−0.5498	−0.2176	0.4959	4.2672	2.0959	4.6282	2.0632	−0.1370
$D3^{[1]}_{\epsilon_A}$	$\sqrt{3}$	$-\sqrt{3}$	$\sqrt{3}$	π	π	π	0	0
$D3^{[2]}_{\epsilon_A}$	2.5425	0	−2.5425	π	π	π	0	0
$T3^{[1]}_{\epsilon_A}$	0	0	0	$\pi/2$	π	$\pi/2$	$\pi/2$	0
$T3^{[2]}_{\epsilon_A}$	0	0	0	$\pi/2$	2π	$\pi/2$	$2\pi/3$	0
$O3^{[1]}_{\epsilon_\Delta\epsilon_A}$	0.8464	−0.1749	0.0990	3.8424	4.6327	6.2041	5.4341	2.7621
$O3^{[2]}_{\epsilon_\Delta\epsilon_A}$	−1.5803	9.1355	−0.1804	7.6803	4.6167	3.8068	0.3477	7.4485
$U3^{[1]}_{\epsilon_\Delta\epsilon_A}$	0	0	0	π	π	π	$\pi/2$	0
$U3^{[2]}_{\epsilon_\Delta\epsilon_A}$	0	0	0	π	π	π	0	π
Short CORPSE	0	0	0	$7\pi/3$	$5\pi/3$	$\pi/3$	π	0
CORPSE	0	0	0	$\pi/3$	$5\pi/3$	$\pi/3$	π	0

In this situation, we have eight free modulation parameters $\{\Delta_n, A_n, \theta_n\}$, $n = 1, 2, 3$. Hence, the cost function can be truncated to ninth order (i.e., $\mathcal{M} = 9$), while the first six order coefficients are used for the constraints. As a result, the optimal problem becomes

$$\min_{\Delta_n, A_n, \theta_n} \mathcal{J}_9 = r^7 a_7^2 + r^8 a_8^2 + r^9 a_9^2,$$
$$\text{such that } a_0 = 1,\ a_1 = a_2 = a_3 = a_4 = a_5 = a_6 = 0. \quad (50)$$

In Table V, we present the modulation parameters of this optimal three-pulse sequence, labeled as the $O3_{\epsilon_A}$ sequence hereafter. The excitation profile is plotted in Fig. 8, as shown by the blue dot-dashed curve.

In Ref. [96], the detuning-modulated CPs are proposed to achieve high-fidelity population transfer by reasonably modulating the detunings while the other parameters remain unchanged. Here, we label the three-pulse sequences in Ref. [96] as the $D3^{[1]}_{\epsilon_A}$ and $D3^{[2]}_{\epsilon_A}$ sequences, which are accurate to fourth and sixth order in the pulse area error ϵ_A, respectively. The corresponding excitation profiles are also plotted in Fig. 8. We can perceive from Fig. 8 that the $O3_{\epsilon_A}$ sequence possesses a broader high-excitation range than the $D3^{[1]}_{\epsilon_A}$ and $D3^{[2]}_{\epsilon_A}$ sequences. The reason is that we not only nullify the first six order coefficients but we further reduce the amplitude of the error coefficients up to ninth order as well. Therefore, the excitation profile for the $O3_{\epsilon_A}$ sequence outperforms the $D3^{[1]}_{\epsilon_A}$ and $D3^{[2]}_{\epsilon_A}$ sequences in terms of robustness.

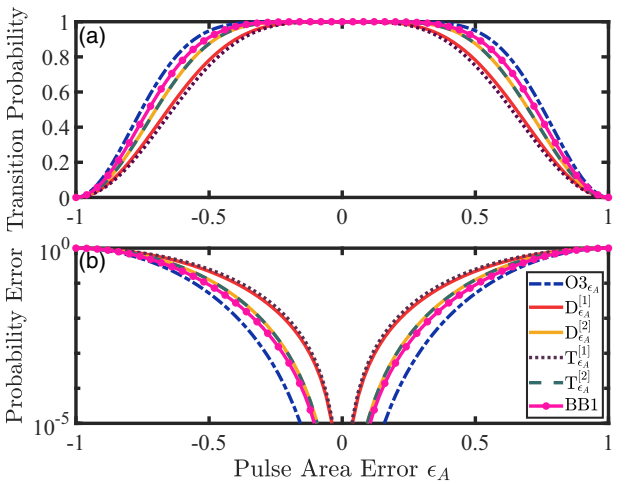

FIG. 8. (a) Excitation profiles for the $O3_{\epsilon_A}$, $D3^{[1]}_{\epsilon_A}$, $D3^{[2]}_{\epsilon_A}$, $T3^{[1]}_{\epsilon_A}$, $T3^{[2]}_{\epsilon_A}$, and BB1 sequences, where the modulation parameters of the first five sequences are given in Table V. (b) Transition probability error $1 - P^{(3)}_{\epsilon_A}$ vs the pulse area error ϵ_A in a logarithmic scale.

The twin composite π-pulse sequence [97], a combination of the normal sequence and its inverted version, is a common phase modulation to efficiently compensate for the pulse area error. In Fig. 8, we also display the excitation profiles for two types of three-pulse twin sequences [97], which are labeled as the $T3^{[1]}_{\epsilon_A}$ and $T3^{[2]}_{\epsilon_A}$ sequences, respectively. Since the $T3^{[1]}_{\epsilon_A}$ and $T3^{[2]}_{\epsilon_A}$ sequences make the transition probability accurate up to $O(\epsilon_A^4)$ and $O(\epsilon_A^6)$, the corresponding excitation profiles are almost similar to the case of the $D3^{[1]}_{\epsilon_A}$ and $D3^{[2]}_{\epsilon_A}$ sequences. As shown in Fig. 8, the current $O3_{\epsilon_A}$ sequence provides the best robustness with respect to the pulse area error among those CPs [96,97].

Finally, we compare the $O3_{\epsilon_A}$ sequence with the BB1 sequence, which is composed of four π pulses with an arbitrary phase χ followed by a θ pulse with zero phase [25]. The form of this sequence can be expressed as

$$\pi_\chi \pi_{3\chi} \pi_{3\chi} \pi_\chi \theta_0, \quad (51)$$

where the subscript represents the phase and $\chi = \arccos(-\theta/4\pi)$. For complete population inversion, we have $\theta = \pi$ and $\chi = \arccos(-1/4)$. It is shown in Fig. 8 that the excitation profile for the BB1 sequence is not as wide as the $O3_{\epsilon_A}$ sequence, since the BB1 sequence is only accurate to $O(\epsilon_A^6)$. Therefore, the current $O3_{\epsilon_A}$ sequence has fewer pulses and is more robust against the pulse area error than the BB1 sequence.

B. Multiple errors

In the presence of the detuning error and the pulse area error, the transition probability of the state $|\psi_2\rangle$ can be expanded

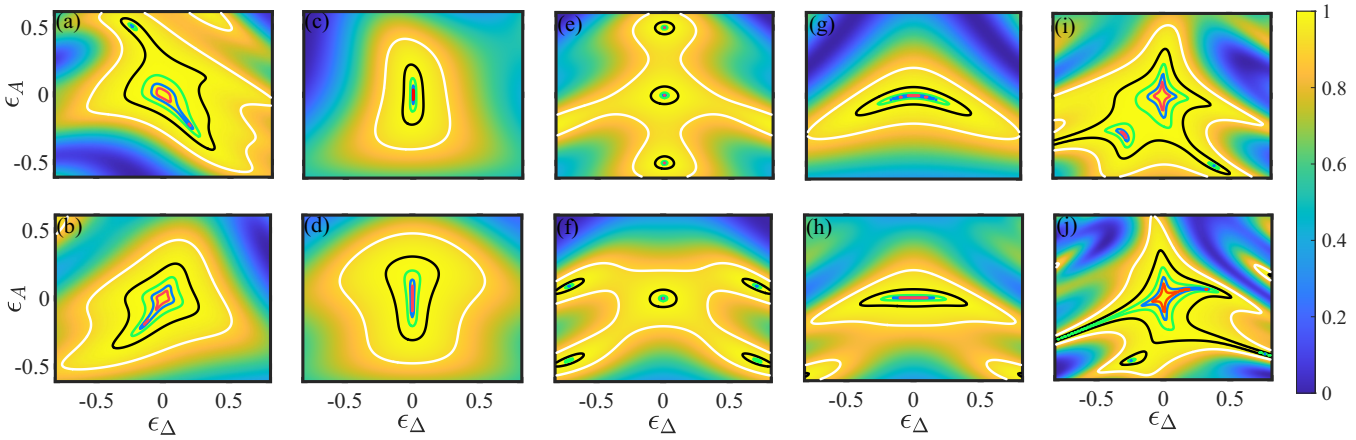

FIG. 9. Transition probability $P^{(3)}_{\epsilon_\Delta\epsilon_A}$ vs the errors ϵ_Δ and ϵ_A in (a) the $\mathrm{O3}^{[1]}_{\epsilon_\Delta\epsilon_A}$ sequence, (b) the $\mathrm{O3}^{[2]}_{\epsilon_\Delta\epsilon_A}$ sequence, (c) the $\mathrm{D3}^{[1]}_{\epsilon_A}$ sequence, (d) the $\mathrm{D3}^{[2]}_{\epsilon_A}$ sequence, (e) the $\mathrm{U3}^{[1]}_{\epsilon_\Delta\epsilon_A}$ sequence, (f) the $\mathrm{U3}^{[2]}_{\epsilon_\Delta\epsilon_A}$ sequence, (g) the short CORPSE sequence, (h) the CORPSE sequence, (i) the reduced CinBB sequence, and (j) the CinBB sequence, where the modulation parameters of the first eight sequences are given in Table V. The white, black, green, blue, and red curves correspond to $P^{(3)}_{\epsilon_\Delta\epsilon_A} = 0.9$, 0.99, 0.999, 0.9999, and 0.99999, respectively (from outside in).

as

$$P^{(3)}_{\epsilon_\Delta\epsilon_A} = a_0 + a_{1,0}\epsilon_\Delta + a_{0,1}\epsilon_A + a_{2,0}\epsilon_\Delta^2 + a_{1,1}\epsilon_\Delta\epsilon_A + a_{0,2}\epsilon_A^2 + a_{3,0}\epsilon_\Delta^3 + a_{2,1}\epsilon_\Delta^2\epsilon_A + a_{1,2}\epsilon_\Delta\epsilon_A^2 + a_{0,3}\epsilon_A^3 + O\big(\epsilon_\Delta^4, \epsilon_\Delta^3\epsilon_A, \epsilon_\Delta^2\epsilon_A^2, \epsilon_\Delta\epsilon_A^3, \epsilon_A^4\big). \tag{52}$$

In this situation, the form of the cost function is

$$\mathcal{J}_3 = r\big(a_{1,0}^2 + a_{0,1}^2\big) + r^2\big(a_{2,0}^2 + a_{1,1}^2 + a_{0,2}^2\big) + r^3\big(a_{3,0}^2 + a_{2,1}^2 + a_{1,2}^2 + a_{0,3}^2\big), \tag{53}$$

where we set $\mathcal{M} = 3$ in Eq. (17).

To see more clearly the difference in robustness of the CPs designed by Eq. (15) and Eq. (22), we individually consider the constraints of the cost function. Specifically, the constraint for Eq. (15) reads

$$a_0 = 1, \tag{54}$$

while it becomes

$$a_0 = 1, \quad a_{1,0} = a_{0,1} = a_{2,0} = a_{1,1} = a_{0,2} = 0, \tag{55}$$

with regard to Eq. (22). For the sake of simplicity, the optimized sequences based on constraints (54) and (55) are labeled as the $\mathrm{O3}^{[1]}_{\epsilon_\Delta\epsilon_A}$ and $\mathrm{O3}^{[2]}_{\epsilon_\Delta\epsilon_A}$ sequences, respectively.

We plot the excitation profiles for both sequences in Figs. 9(a) and 9(b), where the corresponding modulation parameters are listed in Table V. Obviously, the high-excitation region of Fig. 9(a) is much larger than that of Fig. 9(b) (see the white or black curves). This means that the constraint given by Eq. (54) is suitable for the quantum operations with the fidelity being not particularly high. On the contrary, the ultrahigh-excitation region of Fig. 9(b) is larger than that of Fig. 9(a) (see the blue or red curves). The reason is that the low-order coefficients are completely canceled when employing the constraint given by Eq. (55). As a result, the adverse influence on the transition probability mainly originates from the high-order error terms, easily leading to an ultrahigh-excitation region in the presence of tiny errors. In short, both sequences are very robust against the detuning error and the pulse area error. The $\mathrm{O3}^{[1]}_{\epsilon_\Delta\epsilon_A}$ sequence has a larger high-excitation region, while the $\mathrm{O3}^{[2]}_{\epsilon_\Delta\epsilon_A}$ sequence is more efficient for generating ultrahigh excitation.

In Ref. [96], the $\mathrm{D3}^{[1]}_{\epsilon_A}$ and $\mathrm{D3}^{[2]}_{\epsilon_A}$ sequences can also be applicable to compensate for the errors ϵ_Δ and ϵ_A, and the corresponding excitation profiles are plotted in Figs. 9(c) and 9(d). We can see that both sequences are robust against the pulse area error, but with only a slight improvement with respect to the detuning error, as shown by the green (black) curve with a long and narrow peak shape. Compared to the $\mathrm{O3}^{[1]}_{\epsilon_\Delta\epsilon_A}$ and $\mathrm{O3}^{[2]}_{\epsilon_\Delta\epsilon_A}$ sequences, both sequences have an observably smaller high-excitation region, especially for the ultrahigh region [see the blue and red curves in Figs. 9(c) and 9(d)].

Next, we exemplify two kinds of universal CPs [98], labeled as the $\mathrm{U3}^{[1]}_{\epsilon_\Delta\epsilon_A}$ and $\mathrm{U3}^{[2]}_{\epsilon_\Delta\epsilon_A}$ sequences. The former possesses better robustness against the pulse area error, while the latter prefers to compensate for the detuning error. Figures 9(e) and 9(h) show the excitation profiles for these two universal CPs. Because the transition probabilities of these universal CPs are only accurate to second order [98], the high excitation is limited in an extremely small region, enclosed by the green curve in Figs. 9(e) and 9(h). For the ultrahigh-excitation region, they can be almost ignored. In contrast, the high-excitation (ultrahigh-excitation) region is greatly enlarged by the current sequences, as shown in Figs. 9(a) and 9(b). These results firmly verify that the remarkable robustness against multiple types of errors can be also implemented by the current approach.

Another kind of well-known CP is the CORPSE sequence [99] (which stands for compensation for off-resonance with a pulse sequence). Here, we consider two types of them: the CORPSE and the short CORPSE sequences, where the latter has a shorter length (pulse area) in the first pulse. As demonstrated in Figs. 9(g) and 9(h), the excitation profile for the CORPSE sequence performs slightly better than the short one. Furthermore, we can observe in Figs. 9(g) and 9(h) that both sequences have great compensation ability for the detuning error, but are sensitive to the pulse area error [see the transverse region surrounded by the green (blue) curve]. To obtain a better compensation for both the detuning error

and the pulse area error, one can adopt the $O3^{[1]}_{\epsilon_\Delta\epsilon_A}$ and $O3^{[2]}_{\epsilon_\Delta\epsilon_A}$ sequences.

Finally, we turn to the concatenated composite pulses [109], which concatenate different types of CPs to resist multiple errors. For example, to compensate for both the detuning error and the pulse area error, the CORPSE sequence [99] and the BB1 sequence [25] can be concatenated to generate the CinBB (CORPSE in BB1) and the reduced CinBB sequences [100]. Figures 9(i) and 9(j) show the corresponding transition probabilities as a function of the detuning error and the pulse area error, where the reduced CinBB sequence consists of 6 pulses and there are 12 pulses in the CinBB sequence. It can be seen that the robust performance of these two sequences is similar to the $O3^{[1]}_{\epsilon_\Delta\epsilon_A}$ and $O3^{[2]}_{\epsilon_\Delta\epsilon_A}$ sequences. However, we should note that the CinBB and the reduced CinBB sequences have many more pulses than the current one. In particular, as the number of pulses increases, more modulation parameters can be involved in the optimized sequence, leading to a larger area of ultrahigh fidelity.

VI. DISCUSSION AND CONCLUSION

So far, we have placed emphasis on the design of the optimal CP sequence to achieve arbitrary population transfer in a robust way. When further considering the phase of quantum states, it is possible to extend the current method to the implementation of quantum gates. For example, the sequence used for complete population inversion can be directly exploited to implement the X gate by appropriately adjusting the phase of the first pulse. Alternatively, the sequence used for realizing a maximum superposition state can be well adapted to achieve the Hadamard gate. In addition, this method is also available for robust quantum control in multilevel systems. A feasible way is to reduce the multilevel system to an effective two-level one, and then the optimized sequences designed by the current method can be directly applied in the multilevel system. Sometimes, it is deemed insufficient to merely take into account the effective two-level system. In this situation, the pulse design must fully consider the dynamics of all levels in the system, which is reflected in appropriate changes in the construction of the cost function.

In conclusion, we have proposed a general approach of combining the CP technique and the OC theory to achieve optimal robust population transfer in two-level systems. Here, all physical quantities are recognized as modulation parameters in order to reach the efficiency limit in terms of robustness. We focus on reducing the impact of various systematic errors, including the pulse area error, the Rabi frequency error, and the detuning error, on the transition probability. To this end, we use the Taylor expansion to arrange the transition probability into various error terms, and then establish a cost function consisting of the error coefficients and the weighting factor. As a result, the modulation parameters of the CP sequence are obtained by digging out the minimum value of the cost function.

The current approach is quite effective in overcoming the obstacle of incomplete nullification of the error terms of the transition probability or the limited number of pulses. Through adjusting the forms or constraints of the cost function, this approach manifests great flexibility in designing the optimal CPs for different robust performances. Specifically, when changing the form of the cost function, the optimized sequences can be successfully designed for compensating not only the single error but also multiple errors. When adjusting the constraints of the cost function, we also obtain arbitrary population transfer in a robust way. Furthermore, the high-excitation region of the transition probability is adjustable as well, even though many types of errors simultaneously exist in the system. As a by-product, arbitrary robust population transfer can be obtained by only modulating the phase difference of two pulses, effectively reducing the degree of operative difficulty.

Compared with previous CP sequences [96–99], under the same pulse number, the current optimized sequences significantly improve the robustness to the single error as well as the multiple errors. They perform very well in terms of the ultrahigh-excitation region. Furthermore, these optimized sequences also have certain advantages over other sequences [25,100]. More specifically, with fewer pulses, the optimized sequences have a better compensation for the pulse area error than the BB1 sequence [25], and demonstrate a similar robust performance to the CinBB sequences [100]. Therefore, it is believed that this work offers a powerful tool for robust quantum control in quantum information processing.

ACKNOWLEDGMENTS

This work is supported by the Natural Science Foundation of Fujian Province under Grant No. 2021J01575, the Natural Science Funds for Distinguished Young Scholar of Fujian Province under Grant No. 2020J06011, and the Project from Fuzhou University under Grant No. JG202001-2.

[1] M. A. Nielsen and I. L. Chuang, *Quantum Computation and Quantum Information* (Cambridge University Press, Cambridge, UK, 2000).

[2] L. Allen and J. H. Eberly, *Optical Resonance and Two-Level Atoms* (Dover, New York, 1987).

[3] G. S. Vasilev and N. V. Vitanov, Coherent excitation of a two-state system by a linearly chirped Gaussian pulse, J. Chem. Phys. **123**, 174106 (2005).

[4] R. Unanyan, L. Yatsenko, K. Bergmann, and B. Shore, Laser-induced adiabatic atomic reorientation with control of diabatic losses, Opt. Commun. **139**, 48 (1997).

[5] M. V. Berry, Transitionless quantum driving, J. Phys. A: Math. Theor. **42**, 365303 (2009).

[6] X. Chen, I. Lizuain, A. Ruschhaupt, D. Guéry-Odelin, and J. G. Muga, Shortcut to Adiabatic Passage in Two- and Three-Level Atoms, Phys. Rev. Lett. **105**, 123003 (2010).

[7] D. Guéry-Odelin, A. Ruschhaupt, A. Kiely, E. Torrontegui, S. Martínez-Garaot, and J. G. Muga, Shortcuts to adiabaticity: Concepts, methods, and applications, Rev. Mod. Phys. **91**, 045001 (2019).

[8] D. Daems, A. Ruschhaupt, D. Sugny, and S. Guérin, Robust Quantum Control by a Single-Shot Shaped Pulse, Phys. Rev. Lett. **111**, 050404 (2013).

[9] L. Van-Damme, D. Schraft, G. T. Genov, D. Sugny, T. Halfmann, and S. Guérin, Robust NOT gate by single-shot-shaped pulses: Demonstration of the efficiency of the pulses in rephasing atomic coherences, Phys. Rev. A **96**, 022309 (2017).

[10] B. T. Torosov, S. Guérin, and N. V. Vitanov, High-Fidelity Adiabatic Passage by Composite Sequences of Chirped Pulses, Phys. Rev. Lett. **106**, 233001 (2011).

[11] B. T. Torosov, B. W. Shore, and N. V. Vitanov, Coherent control techniques for two-state quantum systems: A comparative study, Phys. Rev. A **103**, 033110 (2021).

[12] Y. B. Band and O. Magnes, Chirped adiabatic passage with temporally delayed pulses, Phys. Rev. A **50**, 584 (1994).

[13] J. S. Melinger, S. R. Gandhi, A. Hariharan, D. Goswami, and W. S. Warren, Adiabatic population transfer with frequency-swept laser pulses, J. Chem. Phys. **101**, 6439 (1994).

[14] N. V. Vitanov, T. Halfmann, B. W. Shore, and K. Bergmann, Laser-induced population transfer by adiabatic passage techniques, Annu. Rev. Phys. Chem. **52**, 763 (2001).

[15] P. Král, I. Thanopulos, and M. Shapiro, Colloquium: Coherently controlled adiabatic passage, Rev. Mod. Phys. **79**, 53 (2007).

[16] N. V. Vitanov, A. A. Rangelov, B. W. Shore, and K. Bergmann, Stimulated Raman adiabatic passage in physics, chemistry, and beyond, Rev. Mod. Phys. **89**, 015006 (2017).

[17] L. P. Yatsenko, S. Guérin, and H. R. Jauslin, Topology of adiabatic passage, Phys. Rev. A **65**, 043407 (2002).

[18] A. Eilam and M. Shapiro, Strong-field adiabatic passage in the continuum: Electromagnetically induced transparency and stimulated Raman adiabatic passage, Phys. Rev. A **85**, 012520 (2012).

[19] S. Guérin, S. Thomas, and H. R. Jauslin, Optimization of population transfer by adiabatic passage, Phys. Rev. A **65**, 023409 (2002).

[20] C. D. West and A. S. Makas, The spectral dispersion of birefringence, especially of birefringent plastic sheets, J. Opt. Soc. Am. **39**, 791 (1949).

[21] G. Destriau and J. Prouteau, Réalisation d'un quart d'onde quasi achromatique par juxtaposition de deux lames cristallines de même nature, J. Phys. Radium **10**, 53 (1949).

[22] S. Pancharatnam, Achromatic combinations of birefringent plates, Proc. Indian Acad. Sci. **41**, 130 (1955).

[23] S. E. Harris, E. O. Ammann, and I. C. Chang, Optical network synthesis using birefringent crystals. I. Synthesis of lossless networks of equal-length crystals, J. Opt. Soc. Am. **54**, 1267 (1964).

[24] C. M. McIntyre and S. E. Harris, Achromatic wave plates for the visible spectrum, J. Opt. Soc. Am. **58**, 1575 (1968).

[25] S. Wimperis, Broadband, narrowband, and passband composite pulses for use in advanced NMR experiments, J. Magn. Reson. Ser. A **109**, 221 (1994).

[26] M. H. Levitt, Composite pulses, Prog. Nucl. Magn. Reson. Spectrosc. **18**, 61 (1986).

[27] S. Wimperis, Iterative schemes for phase-distortionless composite 180° pulses, J. Magn. Reson. **93**, 199 (1991).

[28] B. T. Torosov and N. V. Vitanov, Smooth composite pulses for high-fidelity quantum information processing, Phys. Rev. A **83**, 053420 (2011).

[29] B. T. Torosov and N. V. Vitanov, Arbitrarily accurate variable rotations on the Bloch sphere by composite pulse sequences, Phys. Rev. A **99**, 013402 (2019).

[30] G. T. Genov, D. Schraft, T. Halfmann, and N. V. Vitanov, Correction of Arbitrary Field Errors in Population Inversion of Quantum Systems by Universal Composite Pulses, Phys. Rev. Lett. **113**, 043001 (2014).

[31] N. V. Vitanov, Arbitrarily accurate narrowband composite pulse sequences, Phys. Rev. A **84**, 065404 (2011).

[32] W. Rakreungdet, J. H. Lee, K. F. Lee, B. E. Mischuck, E. Montano, and P. S. Jessen, Accurate microwave control and real-time diagnostics of neutral-atom qubits, Phys. Rev. A **79**, 022316 (2009).

[33] T. Zanon-Willette, R. Lefevre, R. Metzdorff, N. Sillitoe, S. Almonacil, M. Minissale, E. de Clercq, A. V. Taichenachev, V. I. Yudin, and E. Arimondo, Composite laser-pulses spectroscopy for high-accuracy optical clocks: A review of recent progress and perspectives, Rep. Prog. Phys. **81**, 094401 (2018).

[34] G. Demeter, Composite pulses for high-fidelity population inversion in optically dense, inhomogeneously broadened atomic ensembles, Phys. Rev. A **93**, 023830 (2016).

[35] X. Rong, J. Geng, F. Shi, Y. Liu, K. Xu, W. Ma, F. Kong, Z. Jiang, Y. Wu, and J. Du, Experimental fault-tolerant universal quantum gates with solid-state spins under ambient conditions, Nat. Commun. **6**, 8748 (2016).

[36] C. D. Aiello, M. Hirose, and P. Cappellaro, Composite-pulse magnetometry with a solid-state quantum sensor, Nat. Commun. **4**, 1419 (2013).

[37] C. Ventura-Velázquez, B. Jaramillo Ávila, E. Kyoseva, and B. M. Rodríguez-Lara, Robust optomechanical state transfer under composite phase driving, Sci. Rep. **9**, 4382 (2019).

[38] M. Steffen, J. M. Martinis, and I. L. Chuang, Accurate control of Josephson phase qubits, Phys. Rev. B **68**, 224518 (2003).

[39] G. T. Genov, D. Schraft, N. V. Vitanov, and T. Halfmann, Arbitrarily Accurate Pulse Sequences for Robust Dynamical Decoupling, Phys. Rev. Lett. **118**, 133202 (2017).

[40] A. Bruns, G. T. Genov, M. Hain, N. V. Vitanov, and T. Halfmann, Experimental demonstration of composite stimulated Raman adiabatic passage, Phys. Rev. A **98**, 053413 (2018).

[41] S. S. Ivanov and N. V. Vitanov, High-fidelity local addressing of trapped ions and atoms by composite sequences of laser pulses, Opt. Lett. **36**, 1275 (2011).

[42] J. Zhou, S. Li, G.-Z. Pan, G. Zhang, T. Chen, and Z.-Y. Xue, Nonadiabatic geometric quantum gates that are insensitive to qubit-frequency drifts, Phys. Rev. A **103**, 032609 (2021).

[43] Y. Xu, Z. Hua, T. Chen, X. Pan, X. Li, J. Han, W. Cai, Y. Ma, H. Wang, Y. P. Song, Z.-Y. Xue, and L. Sun, Experimental Implementation of Universal Nonadiabatic Geometric Quantum Gates in a Superconducting Circuit, Phys. Rev. Lett. **124**, 230503 (2020).

[44] S. Gulde, S. Gulde, M. Riebe, C. Becher, H. Häffner, H. Eschner, F. Schmidt-Kaler, I. Chuang, and R. Blatt, Implementation of the Deutsch-Josza algorithm on an ion trap quantum computer, Nature (London) **421**, 48 (2003).

[45] F. Schmidt-Kaler, H. Häffner, M. Riebe, S. Gulde, G. Lancaster, T. Deuschle, C. Becher, C. F. Roos, J. Eschner, and R. Blatt, Realization of the Cirac-Zoller controlled-NOT quantum gate, Nature (London) **422**, 408 (2003).

[46] H. Haffner, C. Roos, and R. Blatt, Quantum computing with trapped ions, Phys. Rep. **469**, 155 (2008).

[47] N. Timoney, V. Elman, S. Glaser, C. Weiss, M. Johanning, W. Neuhauser, and C. Wunderlich, Error-resistant single-qubit gates with trapped ions, Phys. Rev. A **77**, 052334 (2008).

[48] T. Monz, K. Kim, W. Hänsel, M. Riebe, A. S. Villar, P. Schindler, M. Chwalla, M. Hennrich, and R. Blatt, Realization of the Quantum Toffoli Gate with Trapped Ions, Phys. Rev. Lett. **102**, 040501 (2009).

[49] C. M. Shappert, J. T. Merrill, K. R. Brown, J. M. Amini, C. Volin, S. C. Doret, H. Hayden, C.-S. Pai, K. R. Brown, and A. W. Harter, Spatially uniform single-qubit gate operations with near-field microwaves and composite pulse compensation, New J. Phys. **15**, 083053 (2013).

[50] E. Mount, C. Kabytayev, S. Crain, R. Harper, S.-Y. Baek, G. Vrijsen, S. T. Flammia, K. R. Brown, P. Maunz, and J. Kim, Error compensation of single-qubit gates in a surface-electrode ion trap using composite pulses, Phys. Rev. A **92**, 060301(R) (2015).

[51] N. V. Vitanov, T. F. Gloger, P. Kaufmann, D. Kaufmann, T. Collath, M. Tanveer Baig, M. Johanning, and C. Wunderlich, Fault-tolerant Hahn-Ramsey interferometry with pulse sequences of alternating detuning, Phys. Rev. A **91**, 033406 (2015).

[52] J. Randall, A. M. Lawrence, S. C. Webster, S. Weidt, N. V. Vitanov, and W. K. Hensinger, Generation of high-fidelity quantum control methods for multilevel systems, Phys. Rev. A **98**, 043414 (2018).

[53] T. Sriarunothai, S. Wölk, G. S. Giri, N. Friis, V. Dunjko, H. J. Briegel, and C. Wunderlich, Speeding-up the decision making of a learning agent using an ion trap quantum processor, Quantum Sci. Technol. **4**, 015014 (2018).

[54] D. L. Butts, K. Kotru, J. M. Kinast, A. M. Radojevic, B. P. Timmons, and R. E. Stoner, Efficient broadband Raman pulses for large-area atom interferometry, J. Opt. Soc. Am. B **30**, 922 (2013).

[55] A. Dunning, R. Gregory, J. Bateman, N. Cooper, M. Himsworth, J. A. Jones, and T. Freegarde, Composite pulses for interferometry in a thermal cold atom cloud, Phys. Rev. A **90**, 033608 (2014).

[56] P. Berg, S. Abend, G. Tackmann, C. Schubert, E. Giese, W. P. Schleich, F. A. Narducci, W. Ertmer, and E. M. Rasel, Composite-Light-Pulse Technique for High-Precision Atom Interferometry, Phys. Rev. Lett. **114**, 063002 (2015).

[57] J. P. Kestner, X. Wang, L. S. Bishop, E. Barnes, and S. Das Sarma, Noise-Resistant Control for a Spin Qubit Array, Phys. Rev. Lett. **110**, 140502 (2013).

[58] C. Zhang, R. E. Throckmorton, X.-C. Yang, X. Wang, E. Barnes, and S. Das Sarma, Randomized Benchmarking of Barrier versus Tilt Control of a Singlet-Triplet Qubit, Phys. Rev. Lett. **118**, 216802 (2017).

[59] G. T. Hickman, X. Wang, J. P. Kestner, and S. Das Sarma, Dynamically corrected gates for an exchange-only qubit, Phys. Rev. B **88**, 161303(R) (2013).

[60] A. P. Peirce, M. A. Dahleh, and H. Rabitz, Optimal control of quantum-mechanical systems: Existence, numerical approximation, and applications, Phys. Rev. A **37**, 4950 (1988).

[61] D. Sugny, A. Keller, O. Atabek, D. Daems, C. M. Dion, S. Guérin, and H. R. Jauslin, Laser control for the optimal evolution of pure quantum states, Phys. Rev. A **71**, 063402 (2005).

[62] C. Brif, R. Chakrabarti, and H. Rabitz, Control of quantum phenomena: Past, present and future, New J. Phys. **12**, 075008 (2010).

[63] K. Kobzar, S. Ehni, T. E. Skinner, S. J. Glaser, and B. Luy, Exploring the limits of broadband 90 and 180 universal rotation pulses, J. Magn. Reson. **225**, 142 (2012).

[64] N. Khaneja, T. Reiss, C. Kehlet, T. Schulte-Herbrüggen, and S. J. Glaser, Optimal control of coupled spin dynamics: Design of NMR pulse sequences by gradient ascent algorithms, J. Magn. Reson. **172**, 296 (2005).

[65] N. Khaneja, R. Brockett, and S. J. Glaser, Time optimal control in spin systems, Phys. Rev. A **63**, 032308 (2001).

[66] T. Caneva, M. Murphy, T. Calarco, R. Fazio, S. Montangero, V. Giovannetti, and G. E. Santoro, Optimal Control at the Quantum Speed Limit, Phys. Rev. Lett. **103**, 240501 (2009).

[67] J. P. Palao and R. Kosloff, Quantum Computing by an Optimal Control Algorithm for Unitary Transformations, Phys. Rev. Lett. **89**, 188301 (2002).

[68] J. P. Palao and R. Kosloff, Optimal control theory for unitary transformations, Phys. Rev. A **68**, 062308 (2003).

[69] G. Gordon, G. Kurizki, and D. A. Lidar, Optimal Dynamical Decoherence Control of a Qubit, Phys. Rev. Lett. **101**, 010403 (2008).

[70] J. Werschnik and E. K. U. Gross, Quantum optimal control theory, J. Phys. B: At. Mol. Opt. Phys. **40**, R175 (2007).

[71] D. Liberzon, *Calculus of Variations and Optimal Control Theory* (Princeton University Press, Princeton, NJ, 2013).

[72] L. S. Pontryagin, V. Boltianski, R. Gamkrelidze, and E. Mitchtchenko, *The Mathematical Theory of Optimal Processes* (Wiley, New York, 1962).

[73] A. Castro and I. V. Tokatly, Quantum optimal control theory in the linear response formalism, Phys. Rev. A **84**, 033410 (2011).

[74] S. J. Glaser, U. Boscain, T. Calarco, C. P. Koch, W. Köckenberger, R. Kosloff, I. Kuprov, B. Luy, S. Schirmer, T. Schulte-Herbrüggen, D. Sugny, and F. K. Wilhelm, Training Schrödinger's cat: Quantum optimal control, Eur. Phys. J. D **69**, 279 (2015).

[75] U. Boscain, M. Sigalotti, and D. Sugny, Introduction to the Pontryagin maximum principle for quantum optimal control, PRX Quantum **2**, 030203 (2021).

[76] P. Kumar, S. A. Malinovskaya, and V. S. Malinovsky, Optimal control of multilevel quantum systems in the field-interaction representation, Phys. Rev. A **90**, 033427 (2014).

[77] I. R. Solá, V. S. Malinovsky, and D. J. Tannor, Optimal pulse sequences for population transfer in multilevel systems, Phys. Rev. A **60**, 3081 (1999).

[78] M. Lapert, Y. Zhang, M. Braun, S. J. Glaser, and D. Sugny, Singular Extremals for the Time-Optimal Control of Dissipative Spin $\frac{1}{2}$ Particles, Phys. Rev. Lett. **104**, 083001 (2010).

[79] X. Chen, E. Torrontegui, D. Stefanatos, J.-S. Li, and J. G. Muga, Optimal trajectories for efficient atomic transport without final excitation, Phys. Rev. A **84**, 043415 (2011).

[80] A. Garon, S. J. Glaser, and D. Sugny, Time-optimal control of SU(2) quantum operations, Phys. Rev. A **88**, 043422 (2013).

[81] L. Van Damme, Q. Ansel, S. J. Glaser, and D. Sugny, Robust optimal control of two-level quantum systems, Phys. Rev. A **95**, 063403 (2017).

[82] T. Fösel, P. Tighineanu, T. Weiss, and F. Marquardt, Reinforcement Learning with Neural Networks for Quantum Feedback, Phys. Rev. X **8**, 031084 (2018).

[83] A. Nagy and V. Savona, Variational Quantum Monte Carlo Method with a Neural-Network Ansatz for Open Quantum Systems, Phys. Rev. Lett. **122**, 250501 (2019).

[84] B. M. Henson, D. K. Shin, K. F. Thomas, J. A. Ross, M. R. Hush, S. S. Hodgman, and A. G. Truscott, Approaching the adiabatic timescale with machine learning, Proc. Natl. Acad. Sci. USA **115**, 13216 (2018).

[85] T. Haug, W.-K. Mok, J.-B. You, W. Zhang, C. E. Png, and L.-C. Kwek, Classifying global state preparation via deep reinforcement learning, Mach. Learn.: Sci. Technol. **2**, 01LT02 (2021).

[86] X.-C. Yang, M.-H. Yung, and X. Wang, Neural-network-designed pulse sequences for robust control of singlet-triplet qubits, Phys. Rev. A **97**, 042324 (2018).

[87] Y. Ding, Y. Ban, J. D. Martín-Guerrero, E. Solano, J. Casanova, and X. Chen, Breaking adiabatic quantum control with deep learning, Phys. Rev. A **103**, L040401 (2021).

[88] S. Husain, M. Kawamura, and J. A. Jones, Further analysis of some symmetric and antisymmetric composite pulses for tackling pulse strength errors, J. Magn. Reson. **230**, 145 (2013).

[89] J. A. Jones, Designing short robust NOT gates for quantum computation, Phys. Rev. A **87**, 052317 (2013).

[90] Z.-C. Shi, H.-N. Wu, L.-T. Shen, J. Song, Y. Xia, X. X. Yi, and S.-B. Zheng, Robust single-qubit gates by composite pulses in three-level systems, Phys. Rev. A **103**, 052612 (2021).

[91] B. T. Torosov and N. V. Vitanov, High-fidelity composite quantum gates for Raman qubits, Phys. Rev. Res. **2**, 043194 (2020).

[92] X. Wang, L. S. Bishop, J. P. Kestner, E. Barnes, K. Sun, and S. D. Sarma, Composite pulses for robust universal control of singlet-triplet qubits, Nat. Commun. **3**, 997 (2013).

[93] X. Wang, L. S. Bishop, E. Barnes, J. P. Kestner, and S. Das Sarma, Robust quantum gates for singlet-triplet spin qubits using composite pulses, Phys. Rev. A **89**, 022310 (2014).

[94] J. Ghosh, S. N. Coppersmith, and M. Friesen, Pulse sequences for suppressing leakage in single-qubit gate operations, Phys. Rev. B **95**, 241307(R) (2017).

[95] C. Zhang, Y. Liu, Z.-C. Shi, J. Song, Y. Xia, and S.-B. Zheng, Robust population inversion in three-level systems by composite pulses, Phys. Rev. A **105**, 042414 (2022).

[96] E. Kyoseva, H. Greener, and H. Suchowski, Detuning-modulated composite pulses for high-fidelity robust quantum control, Phys. Rev. A **100**, 032333 (2019).

[97] B. T. Torosov and N. V. Vitanov, Arbitrarily accurate twin composite π-pulse sequences, Phys. Rev. A **97**, 043408 (2018).

[98] G. T. Genov, M. Hain, N. V. Vitanov, and T. Halfmann, Universal composite pulses for efficient population inversion with an arbitrary excitation profile, Phys. Rev. A **101**, 013827 (2020).

[99] H. K. Cummins, G. Llewellyn, and J. A. Jones, Tackling systematic errors in quantum logic gates with composite rotations, Phys. Rev. A **67**, 042308 (2003).

[100] M. Bando, T. Ichikawa, Y. Kondo, and M. Nakahara, Concatenated composite pulses compensating simultaneous systematic errors, J. Phys. Soc. Jpn. **82**, 014004 (2013).

[101] M. O. Scully and M. S. Zubairy, *Quantum Optics* (Cambridge University Press, Cambridge, UK, 1997).

[102] D. J. Reilly, J. M. Taylor, E. A. Laird, J. R. Petta, C. M. Marcus, M. P. Hanson, and A. C. Gossard, Measurement of Temporal Correlations of the Overhauser Field in a Double Quantum Dot, Phys. Rev. Lett. **101**, 236803 (2008).

[103] X. Hu and S. Das Sarma, Charge-Fluctuation-Induced Dephasing of Exchange-Coupled Spin Qubits, Phys. Rev. Lett. **96**, 100501 (2006).

[104] B. T. Torosov and N. V. Vitanov, Experimental Demonstration of Composite Pulses on IBM's Quantum Computer, Phys. Rev. Appl. **18**, 034062 (2022).

[105] H. L. Gevorgyan and N. V. Vitanov, Ultrahigh-fidelity composite rotational quantum gates, Phys. Rev. A **104**, 012609 (2021).

[106] E. Kyoseva and N. V. Vitanov, Arbitrarily accurate passband composite pulses for dynamical suppression of amplitude noise, Phys. Rev. A **88**, 063410 (2013).

[107] B. T. Torosov, S. S. Ivanov, and N. V. Vitanov, Narrowband and passband composite pulses for variable rotations, Phys. Rev. A **102**, 013105 (2020).

[108] D. Schraft, T. Halfmann, G. T. Genov, and N. V. Vitanov, Experimental demonstration of composite adiabatic passage, Phys. Rev. A **88**, 063406 (2013).

[109] T. Ichikawa, M. Bando, Y. Kondo, and M. Nakahara, Designing robust unitary gates: Application to concatenated composite pulses, Phys. Rev. A **84**, 062311 (2011).